Med12 cooperates with multiple differentiation signals to enhance embryonic stem cell plasticity

Max Fernkorn[1], Christian Schröter[1,*]

[1]Department of Systemic Cell Biology, Max Planck Institute of Molecular Physiology, 44227 Dortmund, Germany

*Correspondence: christian.schroeter@mpi-dortmund.mpg.de

Abstract

Cell differentiation results from coordinated changes in gene transcription in response to combinations of signals. FGF, Wnt, and mTOR signals regulate the differentiation of pluripotent mammalian cells towards embryonic and extraembryonic lineages, but how these signals cooperate with general transcriptional regulators is not fully resolved. Here, we report a genome-wide CRISPR screen that reveals both signaling components and general transcriptional regulators for differentiation-associated gene expression in mESCs. Focusing on the Mediator subunit *Med12* as one of the strongest hits in the screen, we show that it regulates gene expression in parallel to FGF and mTOR signals. Loss of *Med12* is compatible with differentiation along both the embryonic epiblast and the extraembryonic primitive endoderm lineage, but pluripotency transitions are slowed down, and the transcriptional separation between epiblast and primitive endoderm identities is enhanced in *Med12*-mutant cells. These cellular phenotypes correlate with reduced biological noise upon loss of *Med12*. These findings suggest that *Med12* regulates cellular plasticity through the priming of transcriptional changes during differentiation, thereby modulating the effects of a broad range of signals.

Introduction

Cell differentiation during development manifests in expression changes of large gene modules that are triggered by extracellular signals and sequence-specific transcription factors. In response to such stimuli, cells must both be able to faithfully mount complex transcriptional responses, as well as maintain plasticity to be able to adapt to changing environments. Knowledge of the molecular regulators that balance faithful differentiation responses and plasticity is therefore of key importance for a mechanistic understanding of cell differentiation. The earliest cell differentiation events of mammalian embryogenesis first segregate the extraembryonic trophoblast from the inner cell mass (ICM). In a second step, the ICM further differentiates into extraembryonic primitive endoderm (PrE) and the pluripotent embryonic epiblast (Epi), which ultimately forms the fetus (Chazaud & Yamanaka, 2016). Subsequently, epiblast cells transition from the naïve pluripotent state at pre-implantation to formative and then primed pluripotency as they prepare for germ layer differentiation (Kalkan & Smith, 2014; Nichols & Smith, 2009; Smith, 2017). Embryonic stem cells (ESCs) allow modeling both the differentiation towards an extraembryonic PrE identity, as well as transitions between different pluripotent states. Mouse ESCs (mESCs) can either be maintained in medium containing serum and the cytokine LIF, or in a ground state of pluripotency using serum-free N2B27 medium supplemented with LIF and two small molecule inhibitors that activate Wnt/beta-Catenin signaling and inhibit FGF/ERK signaling, respectively (2i + LIF; Ying et al., 2008). Efficient PrE differentiation from mESCs can be achieved from ground state pluripotency by the forced expression of GATA transcription factors together with active FGF/ERK signaling (Fujikura et al., 2002; Schröter et al., 2015; Wamaitha et al., 2015). Transitions between pluripotency states in contrast can be triggered by the removal of small molecule inhibitors from the culture medium alone (Kalkan et al., 2017; Neagu et al., 2020). Together with experiments in the mouse embryo, these stem cell models have provided a comprehensive picture of the signaling control of the early lineage transitions in the mammalian embryo. Both PrE differentiation and exit of epiblast cells from naïve towards formative and primed pluripotency require FGF/ERK signaling as well as Wnt signaling inhibition (Athanasouli et al., 2023; Chazaud & Yamanaka, 2016; Kang et al., 2013; Nichols et al., 2009). PrE differentiation further benefits from LIF signaling (Morgani & Brickman, 2015), whereas the progression of epiblast cells is promoted by the Notch signaling effector RBPJ (Kalkan et al., 2019), and the mTOR signaling effector TFE3 (Betschinger et al., 2013; Villegas et al., 2019).

Developmental signaling systems often culminate in the activation or deactivation of sequence-specific transcription factors. In eukaryotes, transmission of such transcription factor activity changes into altered RNA polymerase activity at specific promoters requires

large multiprotein assemblies such as the Mediator complex that physically bridges between transcription factors and the basal transcriptional machinery (Soutourina, 2018). The mammalian Mediator complex is formed by up to 30 subunits. It can be subdivided into a head, a core and a tail domain, and the transiently associated CDK8 module which consists of four subunits: the CDK8 kinase, CCNC, MED12, and MED13 (Luyties & Taatjes, 2022; Soutourina, 2018). Unperturbed Mediator function is required for expression of most protein-coding genes (Soutourina, 2018). Still, individual Mediator subunits have been linked to transcriptional changes in response to specific signaling systems. Deletion of *Sur2,* which encodes the MED23 subunit, for example abrogates transcriptional activation downstream of ERK-MAPK signaling in mESCs (Stevens et al., 2002). The CDK8 module in particular has been implicated in directing rapid changes in gene expression patterns in response to various stimuli, such as serum stimulation (Donner et al., 2010; Luyties & Taatjes, 2022). Furthermore, CDK8 inhibition in mouse and human ESCs impairs pluripotency exit, mirroring effects of MEK/ERK inhibition (Lynch et al., 2020). MED12, which activates CDK8 function in the kinase module (Knuesel et al., 2009; Park et al., 2018), is essential for axis elongation and the activation of Wnt target genes during mouse development (Rocha et al., 2010). Together, these works suggest that the transmission of specific developmental signals to RNA polymerase II activity can be mapped to specific Mediator subunits. How general these mappings are or whether they are context-dependent is however not clear. It is also not known how interference with Mediator activity in pluripotent cells affects the balance between faithful differentiation lineage plasticity. Here, we aim at identifying factors that mediate transcriptional changes in response to signaling events during early mammalian cell differentiation, using the expression of a *Spry4*$^{H2B\text{-}Venus}$ reporter allele as read-out in a genome-wide CRISPR screen. This reporter is an established indicator of developmental FGF/ERK signals, and its expression is switched on in both Epi and PrE cells during preimplantation development (Morgani et al., 2018). Our screen returns both known and new signaling inputs into *Spry4*$^{H2B\text{-}Venus}$ reporter expression, as well as several components of the Mediator and Elongator complexes. Using epistasis analysis, we demonstrate that *Med12*, one of the strongest hits in the screen, functions independently of and in parallel to the FGF and mTOR signaling systems in pluripotent cells. Functional assays showed that, while not strictly required for lineage transitions, loss of *Med12* leads to impaired signal responsiveness during pluripotency transitions, as well as reduced mRNA levels and noise during extraembryonic cell differentiation. Collectively, these results point to new signal-independent functions of *Med12* that promote cellular plasticity during lineage transitions in early development.

Results

A genome-wide CRISPR screen identifies signaling and transcriptional regulators of *Spry4* expression

The differentiation of pluripotent cells towards different lineages rests on transcriptional changes triggered by extracellular signals. To identify effectors of signal-regulated gene expression during cellular differentiation, we performed a genome-wide CRISPR screen using the expression of a Sprouty4 reporter as a read-out (Hanna & Doench, 2020; Morgani et al., 2018; Fig. 1A). We chose Sprouty4 because it is a known target gene of developmental FGF signals, and shows strong expression changes upon both Epi and PrE differentiation (Morgani et al., 2018; Fig. 1 Supp 1). In serum + LIF medium, the *Spry4* reporter is expressed due to paracrine FGF signals. We generated Cas9-expressing *Spry4*:H2B-Venus reporter cells and transduced them with the Brie gRNA library targeting protein-coding genes (Doench et al., 2016). To identify positive and negative regulators of *Spry4* reporter expression, we flow sorted cells with decreased and increased fluorescence at 6 and 9 days after transduction, and determined enriched guides in sorted fractions (Fig. 1A). We first analyzed perturbations leading to reduced reporter expression. Gene-targeting gRNAs were more strongly enriched in the sorted fractions compared to non-targeting controls (Fig. 1B, Fig. 1 Supp 2, Supp Table 1). We used the robust rank algorithm (RRA; W. Li et al., 2014) to combine information from multiple gRNAs and to rank genes in each of the four conditions (1% and 5% gate at both day 6 and day 9, Supp Table 1). This analysis revealed up to 17 individual genes with an FDR ≤ 0.05, and up to 26 genes with an FDR ≤ 0.2 (Fig. 1C, Fig. 1 Supp 2). We compiled a list of hits by selecting genes that were detected with an FDR of ≤ 0.05 in one condition, or with an FDR of ≤ 0.2 in at least two conditions (Fig. 1D). Protein-protein interaction network analysis with String-DB revealed that most of our hits fell into a small number of groups that were highly connected and associated with specific molecular functions (Szklarczyk et al., 2015; Fig. 1E). One of these groups contained the FGF signaling genes *Fgfr1, Grb2, Sos1,* and *Ptpn11*, as would be expected given the strong regulation of *Spry4* by FGF signaling. Another group contained several genes involved in protein glycosylation and specifically the synthesis of heparan sulfates, such as *Slc35b2*, *Ext1*, *Ext2*, and *Extl3*. Heparan sulfates are crucial co-factors for efficient FGF signaling (Ornitz & Itoh, 2015). Since pooled CRISPR screens detect mainly cell-autonomous functions of gene perturbations, the appearance of these hits indicates that surface-tethered heparan sulfates determine a cell's responsiveness to FGF signaling. Three further groups contained genes associated with ribosome biogenesis and translation (*Rpl9*, *Rpl18*, *Eif3i* and *Dhx37)*, as well as genes of the Elongator (*Elp2 – 6*, *Ikbkap*

and *Kti12*) and Mediator complexes (*Med10, Med12, Med16, Med24* and *Med25*, Fig. 1E), raising the possibility that these factors could have gene- or signal-specific functions in mESCs.

Next, to validate selected hits in an independent experimental setting, and to evaluate their effect size, we knocked out individual candidate genes using the most enriched gRNA from the screen. Since we were interested in mechanisms of transcriptional regulation, we focused on hits related to the Mediator and Elongator complexes, but also included *Grb2* and *Ptpn11* as a reference to evaluate the effects of perturbing FGF signal transduction, and *Sox2* and *Fam98b* as candidates that could not clearly be linked to a functional group (Fig. 1E). Flow cytometry showed that knockout of all tested candidates led to a reduction of mean *Spry4*:H2B-Venus fluorescence levels, albeit to a different degree: Knockout of components of the Elongator complex as well as *Fam98b* and *Sox2* affected Sprouty4:H2B-Venus expression only mildly, whereas knockout of the FGF signaling genes *Grb2* and *Ptpn11* had the strongest effect, although they did not reach the reduction achieved via pharmacological inhibition of FGF signal transduction with the MEK inhibitor PD0325901 (PD03) (Fig. 1F, G). Knockout of Mediator components reduced *Spry4*:H2B-Venus levels to different degrees, with *Med12* having the strongest effect, reducing *Spry4*:H2B-Venus levels to 35.3% ± 1.6% compared to control (Fig. 1F, G). Thus, our screen and validation establish *Med12* as a strong candidate regulator of signal-dependent gene expression in mESCs.

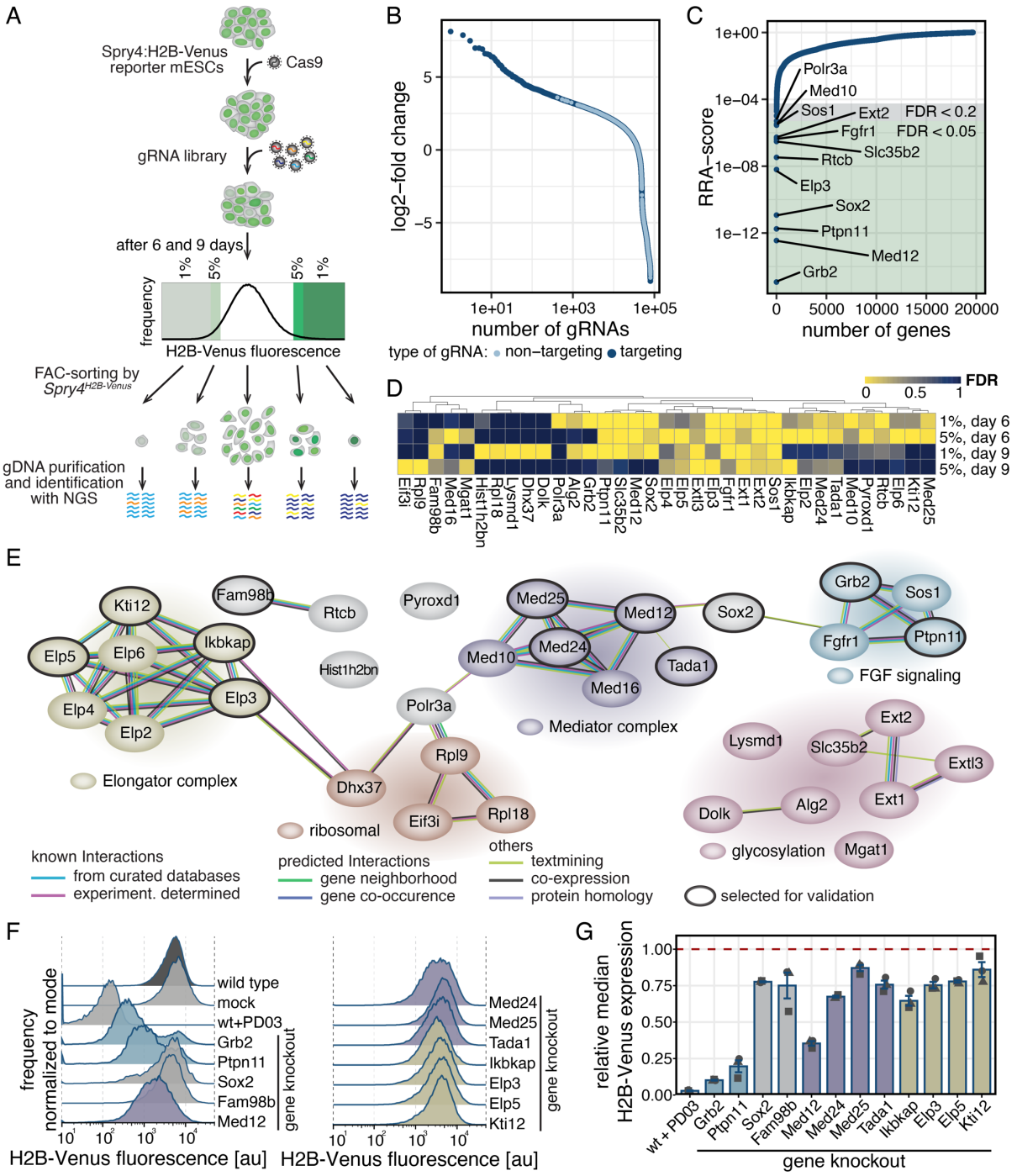

Fig. 1: Genome-wide CRISPR knockout screen reveals positive regulators of Sprouty4 expression.

A Schematic of the pooled CRISPR knockout screen. Cas9-expressing *Sprouty4*$^{H2B\text{-}Venus/+}$ reporter cells were transduced with a genome-wide gRNA library targeting protein-coding genes (Doench et al., 2016). Cells with in- or decreased fluorescence were flow sorted 6 or 9 days after transduction, and gRNAs enriched in sorted populations identified by sequencing.

B, **C** Enrichment of gene-targeting (dark blue) and control gRNAs (light blue) in cells sorted for the lowermost 1% of H2B-Venus signal 6 days after gRNA transduction, displayed as log2-fold change (B) or RRA score of corresponding genes (C). Green and gray background in (C) indicates FDR < 0.05 and < 0.2, respectively.

D Hierarchical clustering of gene perturbations leading to reduced *Spry4*$^{H2B\text{-}Venus}$ expression (FDR ≤ 0.05 in at least one condition or FDR ≤ 0.2 in at least two conditions).
E Protein interaction network of genes shown in (D) based on String-DB. Background colors of genes and gene clusters were manually assigned based on classification by functional similarity.
F, **G** H2B-Venus expression in *Spry4*$^{H2B\text{-}Venus/+}$ reporter cells upon knockout of selected candidate genes 6 d after transfection. (F) shows histograms of one representative experiment, (G) shows mean ± SEM of median H2B-Venus expression from N = 3 independent experiments. $p < 0.05$ for wild type vs. *Elp3*, *Elp5*, *Fam98b*, *Ikbkap*, *Kti12*, *Med25* or *Tada1* knockouts; $p < 0.01$ for wild type vs. *Grb2*, *Med12*, *Med24*, *Ptpn11*, *Sox2* knockouts or PD03-treated cells (Benjamin-Hochberg-adjusted, one-sided, paired t-test).

We next sought to use our screen to identify negative regulators of *Spry4* expression, by looking at perturbations that led to increased reporter expression (Fig. 1A, right side of histogram). Also here, gene-targeting gRNAs were enriched over control guides in the sorted fractions (Fig. 2 Supp 1A-D, Supp Table 1). Ordering according to RRA-scores revealed up to 12 and 24 genes with FDR values of ≤ 0.05 and ≤ 0.2, respectively in each of the conditions (Fig. 2A, Fig. 2 Supp 1E-G, Supp Table 1). Using the same criteria as for the positive regulators, we compiled a list of 29 potential negative regulators of *Spry4* transcription (Fig. 2B). Analysis with String-DB again showed that many of these hits were highly connected and associated with specific molecular functions (Fig. 2C). A large group of genes encoded proteins that localized to mitochondria, or were otherwise associated with mitochondrial functions. Several genes had signaling functions: *Lztr1* is a negative regulator of RAS-MAPK and hence FGF signaling, in line with the strong representation of genes promoting FGF signaling amongst the positive regulators of *Spry4* expression. We detected four genes that were related to mTOR signaling (*Tsc1*, *Tsc2*, *Flcn*, and *Lamtor*). Finally, we found a big group that contained genes involved in chromatin modification and transcription, amongst them three genes encoding SWI/SNF related proteins. Thus, similarly to the collection of positive hits identified above, our screen yields both signaling and transcriptional regulators that negatively control *Spry4* expression. To select hits for validation, we focused on genes associated with mTOR signaling, because these genes have also been implicated in the maintenance of pluripotency (Betschinger et al., 2013; M. Li et al., 2018; Villegas et al., 2019). We also included *Lztr1* as an FGF signaling gene, and *Smarcc1* as a representative of the group of chromatin modifiers. Knockout of all six individual candidate genes with single gRNAs led to an increase of mean *Spry4*:H2B-Venus fluorescence levels in reporter cells. The effect of knocking out the mTOR signaling genes was stronger than that of knocking out *Lztr1* or *Smarcc1*, and almost doubled reporter expression levels compared to mock-transfected cells (Fig. 2D, E).

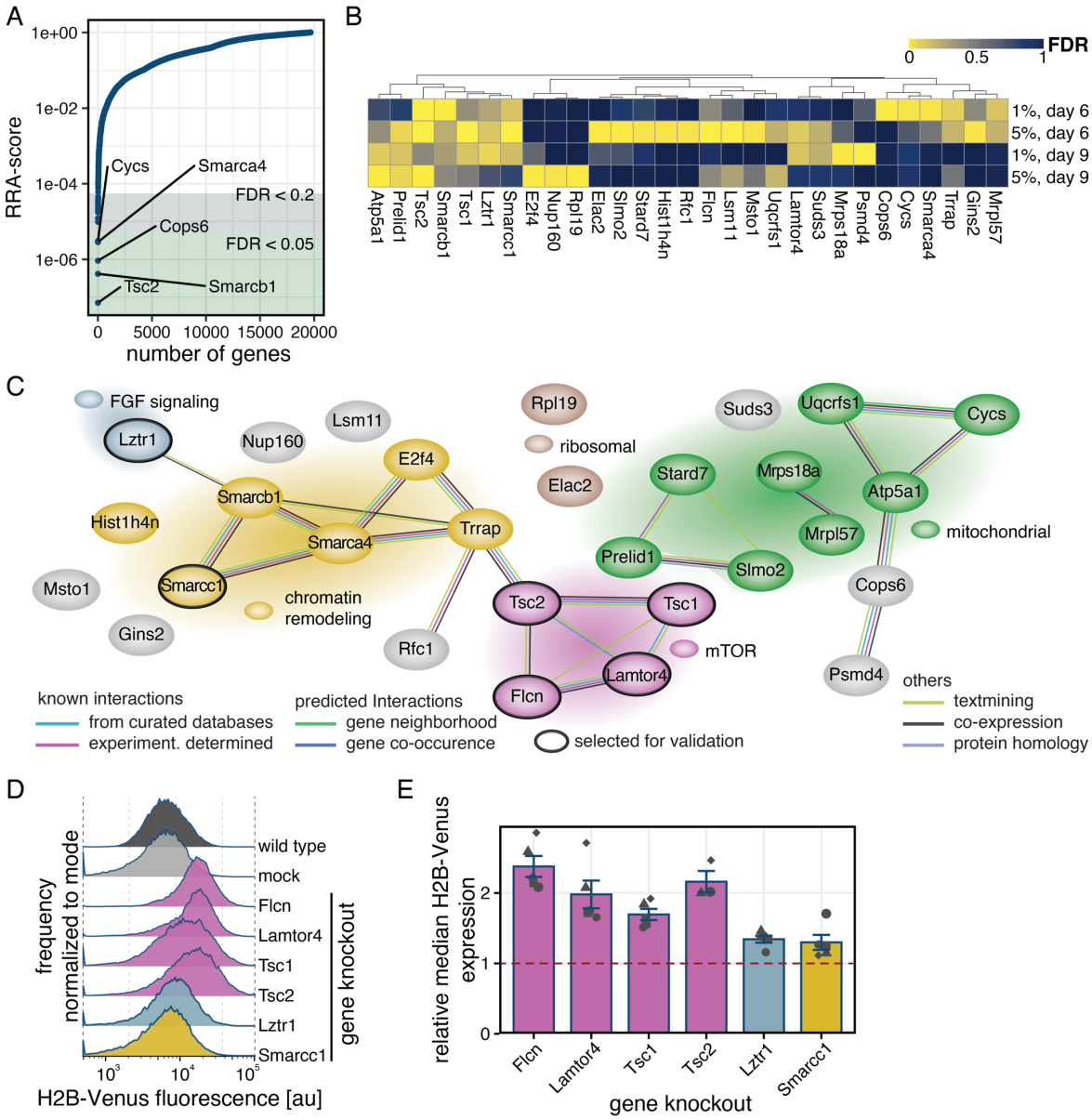

Fig. 2: Genome-wide CRISPR knockout screen reveals negative regulators of Sprouty4 expression.

A RRA scores of genes corresponding to gRNAs enriched in cells sorted for the topmost 1% of H2B-Venus signal on day 6 after gRNA transduction.

B Hierarchical clustering of gene perturbations leading to increased *Spry4*$^{H2B\text{-}Venus}$ expression (FDR ≤ 0.05 in at least one condition or FDR ≤ 0.2 in at least two conditions).

C Protein interaction network of genes shown in (B) based on String-DB. Background colors of genes and gene clusters were manually assigned based on classification by functional similarity.

D, **E** H2B-Venus expression in *Spry*$^{H2B\text{-}Venus/+}$ reporter cells upon knockout of selected candidate genes 6 d after transfection. (D) shows histograms of one representative experiment, (E) shows mean ± SEM of median H2B-Venus expression, N ≥ 3 independent experiments. $p < 0.05$ for mock-transfected wild type vs. *Smarcc1* knockout; $p < 0.01$ for mock-transfected wild type vs. all other knockouts (Benjamin-Hochberg-adjusted, one-sided, paired t-test).

Med12 regulates gene expression in mESCs independently from pluripotency-related signaling pathways

We then wanted to know how the signaling and transcriptional regulators identified in the CRISPR-screen were functionally related. We focused on *Med12*, since of all transcriptional regulators, it had the strongest effect on *Spry4* reporter expression. Furthermore, MED12 is a component of Mediator's kinase module which could couple the activities of specific signaling systems to transcriptional activity (Lynch et al., 2020; Rocha et al., 2010). To analyze *Med12* functions in mESCs, we first generated monoclonal *Med12*-mutant cell lines. We removed part of exon 7, a region that was also targeted by sgRNAs used in the CRISPR-screen, and confirmed the loss of MED12 protein expression by immunoblotting (Fig. 3 Supp 1A, B). *Med12*-mutant cells grew normally in both serum + LIF and 2i + LIF medium, and showed a reduced increase in *Spry4* reporter expression upon switching from 2i + LIF to the N2B27 base medium (Fig. 3 Supp 1C, D). ppERK levels were indistinguishable between wild-type and *Med12*-mutant lines (Fig. 3 Supp 1E, F), indicating that reduced *Spry4* reporter expression is not due to deregulated FGF/ERK signaling.

To assess global gene expression differences between wild-type and *Med12*-mutant cells, we performed bulk RNA sequencing of cells in 2i medium and upon 24 h of differentiation in N2B27 (Fig. 3A). Principal component analysis separated samples in pluripotency and differentiation medium along PC1 (32.1% of variance), and wild-type and *Med12*-mutant cells along PC2 (16.8% of variance, Fig. 3B). Fewer genes were differentially expressed between pluripotency conditions and 24 h in N2B27 in *Med12*-mutant compared to wild-type cells. Most genes that were differentially expressed in the mutant were also differentially expressed in the wild type (Fig. 3C, left, Supp Table 2). When comparing between wild-type and *Med12*-mutant cells within each culture condition, we found that more genes were differentially expressed between the two genotypes in N2B27 than in 2i (Fig. 3C, right, Supp Table 2). Thus, loss of *Med12* impairs gene expression changes at the exit from pluripotency. *Med12* has a closely related paralogue named *Med12l*. *Med12l* expression was upregulated in *Med12*-mutant cells (Fig. 3 Supp 2A), and *Spry4* reporter expression in *Med12*-mutant lines could be further reduced by simultaneously knocking-out *Med12l* (Fig. 3 Supp 2B). Thus, it is possible that *Med12l* partially compensates for loss of *Med12* function in the mutant lines.

Exit from pluripotency is regulated by the interplay of a set of signaling systems, such as mTOR, Notch, Wnt, and FGF (Betschinger et al., 2013; Kalkan et al., 2019; Ying et al., 2008). We next asked if gene expression downstream of any of these signaling systems was affected by loss of *Med12*, using previously defined sets of target genes specific for each signaling system (Lackner et al., 2021). A strong expression change of such a set of target genes

between wild type and mutant cells can be considered a footprint of the perturbation of the corresponding signaling system. In *Med12* mutant cells, this gene expression footprint was strongest for mTOR target genes, less pronounced for Notch and Wnt target genes, and virtually absent for FGF target genes (Fig. 3D). We functionally tested the relationship between *Med12* and mTOR signaling by knocking out the mTOR signaling genes *Flcn*, *Lamtor4*, *Tsc1* and *Tsc2* in *Med12*-mutant *Spry4*$^{H2B\text{-}Venus/+}$ cells. Similarly to the situation in the wild type, knockout of these genes led to increased reporter expression, albeit from a lower baseline level (Fig. 3E). Therefore, *Med12* regulates *Spry4* expression independently from mTOR signaling. In addition to mTOR signaling genes and Mediator subunits, our CRISPR screen revealed a large number of genes involved in FGF signal transduction, but the footprinting analysis suggested that FGF inputs into gene expression were independent from *Med12*. To further corroborate this result, we generated *Med12* mutations in the background of an *Fgf4*-mutant mESC line, which allowed us to specifically analyze the effects of FGF signaling upon the switch from pluripotency to differentiation medium. We wanted to focus on immediate gene expression changes triggered by FGF signaling, and therefore analyzed gene expression changes by bulk RNA-sequencing after 6 h of transfer into N2B27 medium with or without addition of exogenous FGF (Fig. 3F). Again, principal component analysis showed that cells in pluripotency and differentiation medium were separated along PC1 (33.2% of variance), and wild-type and *Med12*-mutant cells separated along PC3 (9.3% of variance), both when analyzing independent *Med12*-mutant clonal cell lines as well as experimental replicates (Fig. 3G). If expression of FGF target genes was generally dependent on *Med12,* we would expect that their fold-change is lower in *Med12*-mutant compared to wild-type cells. However, when plotting the fold expression-change for each gene upon 6 h of FGF stimulation for wild-type versus *Med12*-mutant cells, we found that the majority of genes were induced to a similar degree in both genotypes (2006 genes), while only 926 and 935 genes were differentially expressed in the wild-type or the *Med12*-mutant only (Fig. 3H, Supp Table 3). Furthermore, the ratios of fold-change values of FGF target genes between *Med12*-mutant and wild-type cells showed a unimodal distribution with a mode of 1.068 for downregulated and 0.927 for upregulated genes (Fig. 3J). While this slight deviation of the mode from 1 leaves open the possibility that *Med12* influences their expression magnitude, overall these results argue against a strong and specific role of *Med12* in the regulation of FGF target genes.

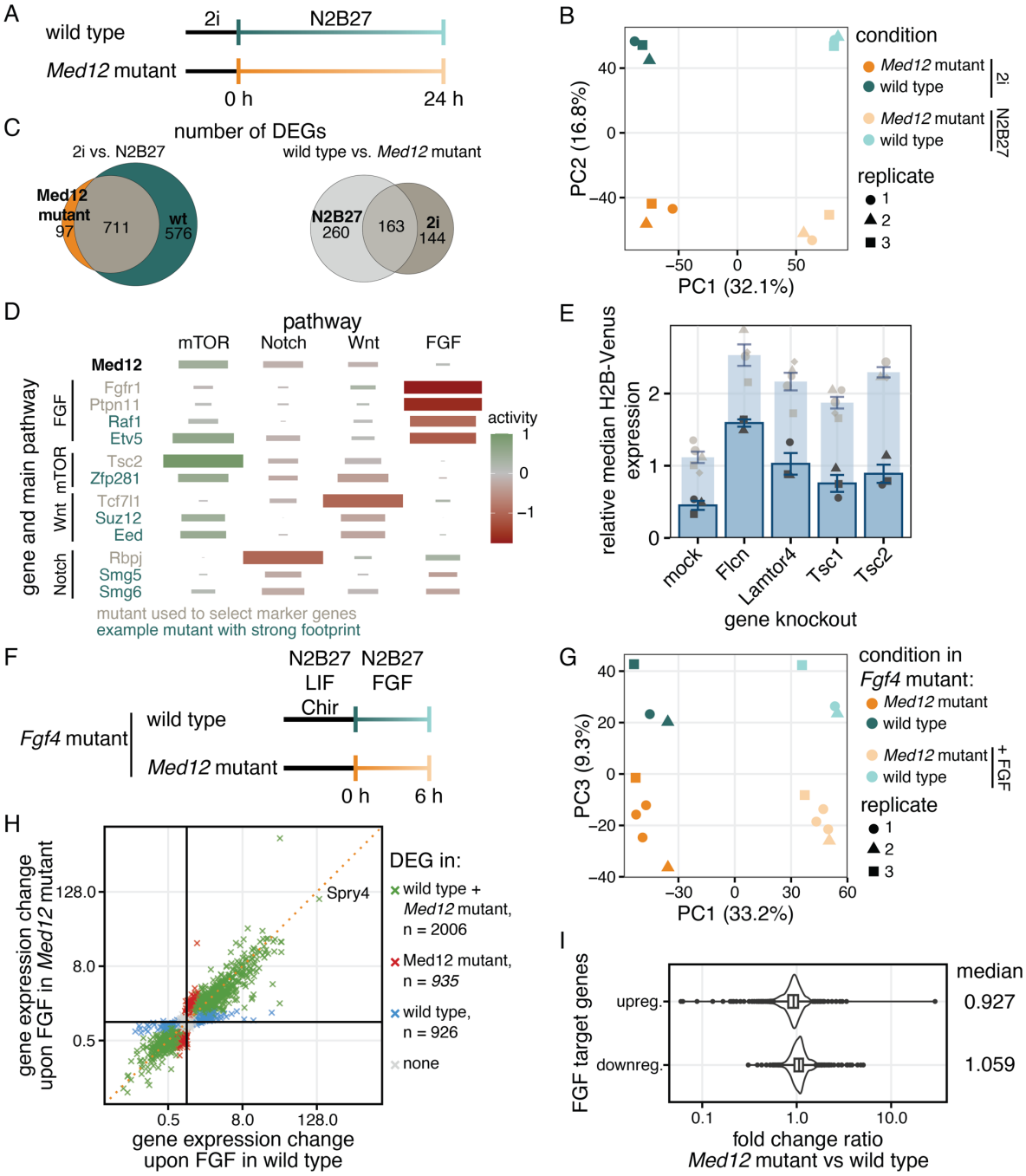

Fig. 3: *Med12* affects gene expression independently of pluripotency related signaling systems.

A Schematic of experiment to identify *Med12*-regulated genes by bulk RNA sequencing.

B Principal component analysis transcriptomes from (A).

C Euler-diagram showing the number differentially expressed genes (log2-fold change > |1|, adjusted p-value < 0.01) in bulk transcriptomes. Left panel compares genes differentially expressed upon 24 h of differentiation between *Med12*-mutant and wild-type cells, right panel compares genes differentially expressed upon loss of *Med12* between N2B27 and 2i.

D Expression footprint analysis using a set of 50 marker genes per pathway defined in (Lackner et al., 2021). Top row shows footprint of *Med12*-mutant cells. Lower rows show expression footprints of mutants from Lackner et al., 2021, for comparison. Gray: Mutants that were used to select marker genes. Green: Independent example mutants that show a strong and specific footprint of one of the

pathways. Tile color indicates relative pathway activity, tile size indicates spearman correlation of footprint genes with pathway-defining mutants.

E Median H2B-Venus fluorescence upon mutation of mTOR related genes in *Med12*-mutant *Spry4*$^{H2B\text{-}Venus/+}$ cells, normalized to H2B-Venus expression in *Med12* wild-type cells. Median H2B-Venus fluorescence upon mutation of mTOR related genes in *Med12* wild-type cells is reproduced from Fig. 2E for comparison (light blue). Error-bars indicate SEM, points individual replicates, N ≥ 3 independent experiments.

F Schematic of experiment to test *Med12*-dependency of FGF target genes by RNA sequencing.

G Principal component analysis transcriptomes from (F). PC2 (not shown; 12.8% of variance) separated experimental replicates from each other.

H Gene expression changes and number of significantly differentially expressed genes (adjusted p-value < 0.01) upon FGF4 stimulation in wild-type versus *Med12*-mutant cells. Dotted orange line indicates the unity line.

I Ratio of fold changes for FGF target genes between wild-type and *Med12*-mutant cells, for up- (top) and downregulated genes (bottom). FGF target genes were defined as having a log2-fold change in wild-type cells upon FGF4 stimulation > |1| and an adjusted p-value < 0.05.

Med12 regulates naïve pluripotency

We then asked if altered gene expression in the *Med12* mutants had any functional consequences. To probe exit from naïve pluripotency, we performed a colony formation assay (Kalkan et al., 2017), where we differentiated cells in N2B27 for 48 h, followed by seeding at clonal density in 2i + LIF medium (Fig. 4A). Because we grew cells in the presence of LIF before transfer into N2B27, wild-type cells still formed a large number of pluripotent colonies (Lackner et al., 2021). In *Med12*-mutant cells in contrast, the number of pluripotent colonies was significantly reduced. (Fig. 4B, left, Fig. 4 Supp 1A, Supp Table 4). To test how this phenotype related to FGF signaling, we carried out the same colony differentiation assay in an *Fgf4* mutant background. When differentiated for 48 h in N2B27, *Med12* wild-type and mutant cells formed a similar number of colonies upon transfer to pluripotency medium. Upon supplementation of N2B27 with FGF4, the number of pluripotent colonies formed by *Fgf4; Med12* double mutant cells was much reduced, both compared to the *Fgf4* single mutant supplemented with FGF4, and the *Fgf4; Med12* double mutant in the absence of FGF4 (Fig. 4B, right, Fig. 4 Supp 1B). Thus, this experiment corroborates our conclusion from the transcriptomic analysis that Med12 cooperates with FGF signaling at the exit from pluripotency.

The ability to form pluripotent colonies in the colony formation assay depends on a cell's pluripotency state at the beginning of the differentiation period, and its ability to react to changing culture conditions. We used our bulk RNA sequencing data comparing wild-type and

Med12-mutant cells after 24 h in N2B27 to evaluate which of these properties were affected upon loss of *Med12*. We first determined differentiation delays of the two genotypes using a published high time-resolution reference dataset (Lackner et al., 2021). Surprisingly, this analysis indicated that *Med12*-mutant cells differentiated more slowly than the wild-type (Fig. 4C). This could be a consequence of stronger expression of naïve genes in pluripotency conditions, or reflect slower downregulation of these genes in N2B27 in the *Med12* mutant. To distinguish between these possibilities, we plotted the expression levels of 7 selected pluripotency marker genes in 2i and after 24 h in N2B27 in wild-type versus *Med12*-mutant cells. In this plot, data points above and below the unit line indicate higher and lower expression in the mutant relative to the wild type, respectively, and the slope of the connecting line between expression in 2i and N2B27 indicates the dynamics of down-regulation (Fig. 4D, left). We found that in 2i medium, all marker genes were less strongly expressed in the mutant compared to the wild type. Furthermore, their slopes were consistently smaller than one (Fig. 4D). Such a systematic reduction in the slope of downregulation was also observed when we analyzed the top 100 downregulated genes in wild-type or *Med12*-mutant cells (Fig. 4E). These findings suggest that *Med12*-mutant cells both have impaired pluripotency gene expression in 2i, as well as a reduced ability to react to changing culture conditions. In the colony formation assay, cells need to re-establish pluripotency gene expression. We therefore surmise that the reduced colony formation capacity of *Med12*-mutant cells in the colony formation assay is dominated by their reduced ability to react to changing culture conditions.

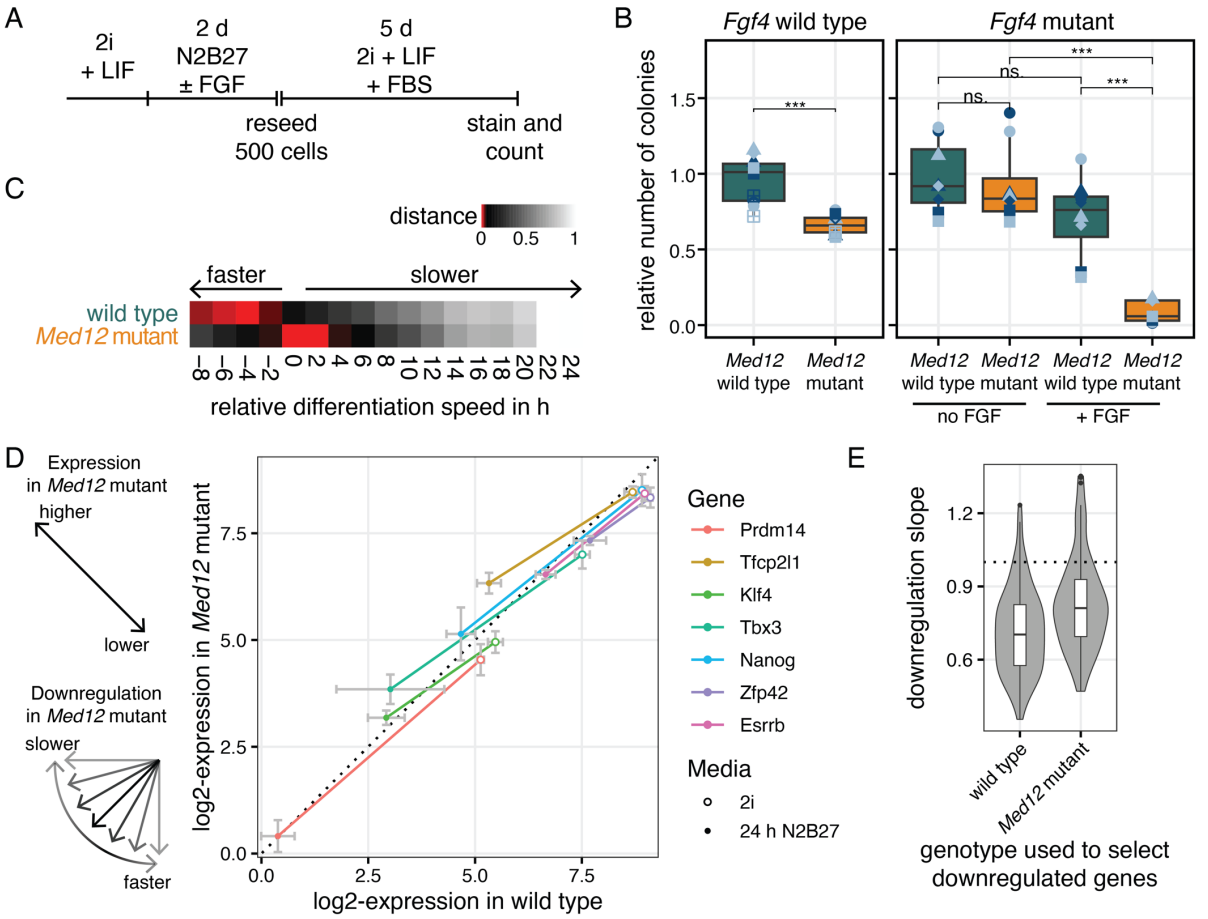

Fig. 4: Mutation of *Med12* affects the exit of pluripotency.

A Experimental approach to determine clonogenicity of *Med12*-mutant and wild-type cells. 2i + LIF was supplemented with FBS to support growth of *Fgf4*-mutant cells after reseeding.

B Number of colonies after treatment as indicated in (A) for both wild-type and *Med12*-mutant cells in an *Fgf4* wild-type (left) and *Fgf4* mutant background with and without supplementation with 10 ng/µL FGF4 (right). N ≥ 4 independent experiments, same symbols in different colors indicate technical replicates within an independent experiment. ns indicates p ≥ 0.05, *** indicates p ≤ 0.001, paired Wilcoxon signed rank test.

C Estimation of differentiation delay in wild-type and *Med12*-mutant cells, relative to a published time resolved gene expression dataset (Lackner et al., 2021). Plot shows the normalized Euclidean distance of the expression of naïve marker gene panel (*Prdm14*, *Tfcp2l1*, *Klf4*, *Tbx3*, *Nanog*, *Zfp42*, *Esrrb*) to the reference dataset. The negative delay values for our wild-type cells likely reflect small differences in experimental design compared to the study by (Lackner et al., 2021).

D Expression of naïve pluripotency marker genes in 2i (open circles) and after 24 h differentiation in N2B27 (dots) in wild-type versus *Med12*-mutant cells. Relative expression values shown as log2(TPM), error bars indicate standard deviation.

E Distribution of downregulation slopes determined as in **D** for the 100 genes with the strongest negative fold-change in wild-type (left) and *Med12*-mutant cells (right). Bar indicates median, boxes indicate 25th and 75th percentile.

Transition between embryonic and extraembryonic identities is buffered against loss of *Med12*

We next sought to further probe the role of *Med12* in an experimental system where the doxycyclin-induced expression of GATA factors brings ground state pluripotent cells into an ICM-like state, from which they can differentiate towards the Epi identity marked by NANOG expression, or the PrE identity marked by the expression of endogenous GATA factors and SOX17 (Fig. 5A; Schröter et al., 2015). We used PiggyBac transgenesis to establish new cell lines carrying inducible GATA6-mCherry constructs, and mutated *Med12* in this background to determine if it is required for PrE differentiation. After an 8 h doxycycline pulse followed by 20 h of differentiation in N2B27 medium, a mix of SOX17-positive PrE cells and NANOG-positive Epi cells differentiated irrespective of *Med12* status, but the fraction of PrE cells was lower, and that of Epi cells was higher in mutant compared to wild-type cultures (Fig. 5B, C). This difference in ratios was maintained even upon supplementation of exogenous FGF during the differentiation phase, suggesting that the lowered PrE differentiation propensity upon loss of *Med12* is not due to lowered FGF signaling in the mutant cultures (Fig. 5 Supp 1A).

PrE differentiation requires the expression of inducible GATA factors above a threshold level (Schröter et al., 2015). We therefore assessed transgene induction levels in *Med12* mutant cells, and found that they were reduced in independent clonal inducible lines (Fig. 5D). To test if *Med12* mutant cells had an altered GATA induction threshold for PrE differentiation, we performed time-lapse imaging of inducible GATA6-mCherry expression followed by fixation and staining for fate markers (Schröter et al., 2015). We attempted to equalize induction levels by reducing the induction time in wild-type cells to 4 h, while inducing *Med12*-mutant cells for 8 h in 2i + LIF medium. The mutant cells showed a longer delay between doxycycline addition and the appearance of GATA6-mCherry fluorescence, and GATA6-mCherry expression levels rose more slowly than in the wild type. Furthermore, GATA6-mCherry levels continued to rise for approximately 2 h after doxycycline removal in wild-type but not in *Med12*-mutant cells (Fig. 5E, Supp Movie 1). These altered induction dynamics point to a critical role of *Med12* for efficient transgene expression.

Connecting inducible GATA expression with differentiation outcome in individual cells revealed that low and high inducible GATA6-mCherry expression in *Med12* mutants were associated with Epi and PrE differentiation, respectively, similar to the situation in wild-type cells (Fig. 5F, G; Schröter et al., 2015). We applied receiver operating characteristics to test how well differentiation could be predicted based on a GATA6-mCherry expression threshold, and to determine the value of an optimal threshold (Fawcett, 2006). GATA6-mCherry expression levels had similar predictive power for differentiation outcome in wild-type and

Med12-mutant cells as judged by plotting the area under the curve (AUC) over time (Fig. 5H). When comparing optimal threshold values, we found that these tracked overall GATA6-mCherry expression levels and were thus slightly lower in *Med12*-mutant cells (Fig. 5I). This indicates that altered proportions of Epi and PrE cells upon loss of *Med12* are largely due to reduced transgene induction levels and not to a reduced ability for PrE differentiation. This conclusion was further supported by flow sorting wild-type and Med12-mutant cells with high GATA6-mCherry expression levels (Fig. 5 Supp 1 C, D). Disruption of cell-cell interactions upon sorting and reseeding resulted in low PrE differentiation in N2B27 medium (Raina et al., 2021), but supplementation of exogenous FGF4 rescued PrE differentiation to similarly high levels in both wild-type and *Med12*-mutant cells (Fig. 5 Supp 1 D, E). Taken together, these experiments suggest that although *Med12* plays important roles for the efficient expression of individual genes, the transition between embryonic and extraembryonic identities is to a large degree buffered against loss of *Med12*.

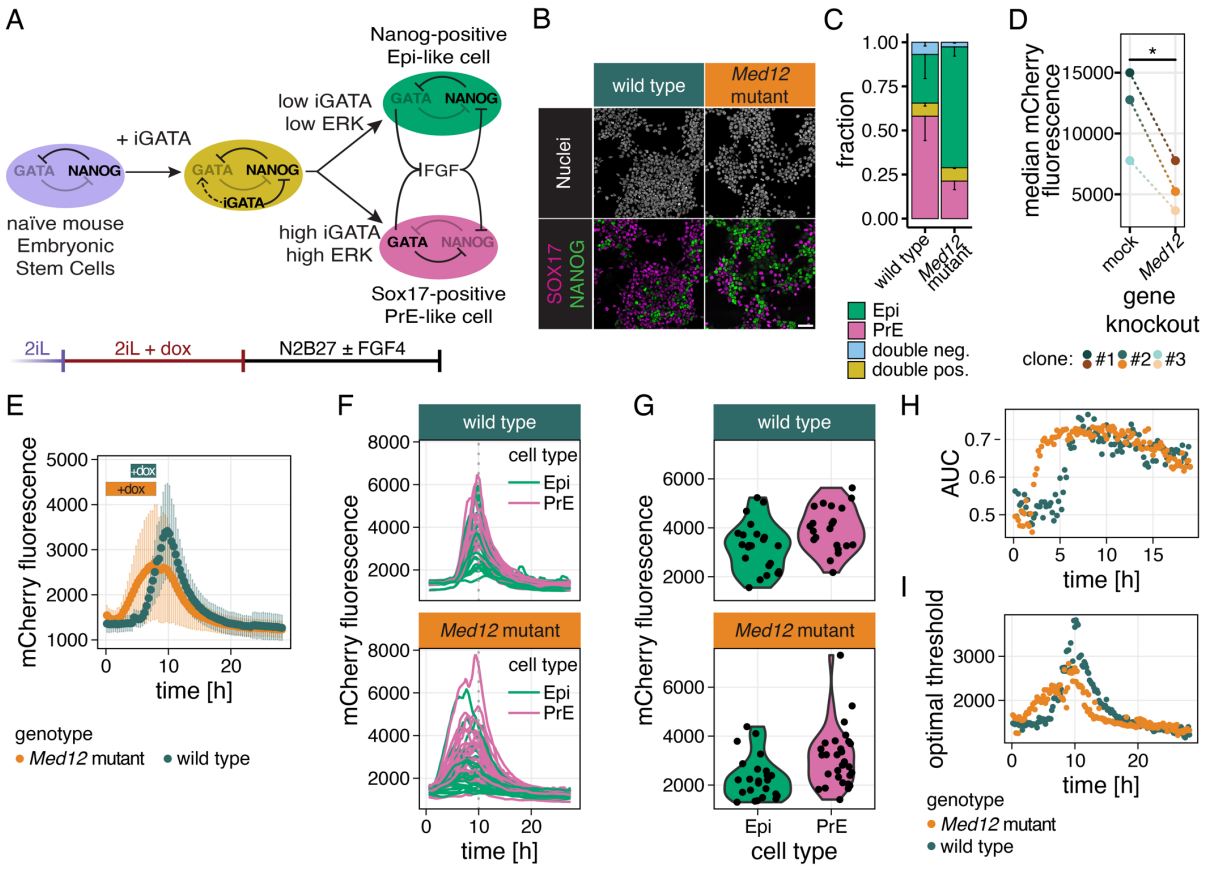

Fig. 5: Transition between embryonic and extraembryonic identities is buffered against loss of *Med12*.

A Schematic of experimental approach to model differentiation of mESCs towards epiblast and primitive endoderm via GATA induction.

B Immunostaining for the Epi-marker NANOG (green) and the PrE marker SOX17 (magenta) after 8 h of GATA6 induction followed by 20 h of differentiation in wild-type and *Med12*-mutant cells. Scale bar: 50 µm.

C Quantification of cell type proportions after differentiating wild-type and *Med12*-mutant cells as in (B). N = 3, n > 1100 cells per replicate, error bars indicate SEM.

D Median Gata6-mCherry fluorescence upon 8h dox induction in three independent clonal GATA6-mCherry inducible cell lines 7 days after transfection with control or *Med12*-targeting gRNAs. * indicates $p \leq 0.05$, paired student's t-test.

E Quantification of Gata6-mCherry expression dynamics from time-lapse movies during induction and differentiation. Boxes indicate induction times (8 h for *Med12* mutant, 4 h for wild type). Error bars indicate SD. One out of N = 5 replicates shown, n > 300 cells per time point.

F Same experiment as in (E), but showing Gata6-mCherry fluorescence in single cells. Trace color indicates differentiation outcome determined by immunostaining (Epi: green; PrE: magenta).

G Gata6-mCherry fluorescence in single cells 2 h after the end of induction, plotted separately for prospective Epi and PrE cells.

H Predictive power of GATA6-mCherry expression determined as Area Under the Curve (AUC) from ROC-analysis.

I Optimal GATA6-mCherry threshold to predict differentiation outcome determined by Youden's J statistic of ROC-analysis.
F - **I** Data from one representative experiment out of N = 3 replicates, n ≥ 45 cells per genotype.

Loss of *Med12* reduces biological noise

Finally, we performed single-cell sequencing to determine how Med12 shapes the global transcriptional signature of PrE differentiation. Multiplexing and pooling of samples before mRNA capture and library preparation allowed us to minimize batch effects, and to generate sample replicates using independent *Med12* wild type and mutant cell lines (Fig. 6A). As in previous experiments, we induced GATA transgenes for 4 h in wild-type and 8 h in *Med12*-mutant cells, and started differentiation simultaneously in both genotypes by switching from 2i + LIF medium to N2B27. In a UMAP representation of transcriptomes from all ten samples, cells from pluripotency and differentiation conditions formed two coherent groups, respectively. Within each of the groups, wild type and *Med12*-mutant cells segregated from each other (Fig. 6B). Cells from differentiation conditions were negative for the Wnt/β-Catenin target *Sp5* and positive for the differentiation marker *Dnmt3l*, while PrE markers *Sox17, Dab2*, and *Cubn* and the Epi markers *Nanog* and *Fgf4* showed a mutually exclusive expression pattern, indicative of the split between the two lineages (Fig. 6C). To evaluate the consequences of loss of *Med12* in this experiment, we next analyzed pluripotency and differentiation samples separately, and used principal component analysis as a means to graphically preserve quantitative differences in gene expression between cells. In pluripotency conditions, single cell transcriptomes from wild-type and *Med12*-mutant cells were clearly separated, demonstrating that loss of *Med12* leads to a globally consistent shift of gene expression state (Fig. 6D). Consistent with our results from bulk RNA sequencing, expression levels of the pluripotency genes *Klf4*, *Zfp42*, and *Tbx3* were reduced in the mutant cells, whereas levels of *Prdm14*, *Nanog*, *Esrrb*, and *Tcf21l1* were similar between the two genotypes (Fig. 6E). Next, we exploited our multiplexed dataset to ask if loss of *Med12* changes mRNA levels in cells. In pluripotency conditions, the number of mRNAs captured from wild-type and *Med12*-mutant cells was not significantly different (median number of UMIs 24437 and 23806, respectively). Differentiation resulted in an increased number of captured mRNAs in both genotypes, with wild-type cells expressing significantly more mRNAs than *Med12* mutants (median number of UMIs 28227 and 25649, respectively, Fig. 6E). This suggests that *Med12* enhances global transcriptional output during differentiation.

We then asked how loss of *Med12* affected the separation between Epi and PrE identities. To consistently identify Epi and PrE cells across genotypes, we integrated the five differentiated samples and clustered them to separate two major groups across the integrated dataset (Fig.

6G). In principle component space, these two groups were separated along PC1 (Fig. 6G). Cluster 0 was characterized by the expression of PrE marker genes such as *Gata6*, while cluster 1 expressed Epi markers such as *Nanog* (Fig. 6 H, Supp Table 5). The proportions of the two cell types captured by these clusters differed with *Med12* genotype: In the two wild-type cell lines, 60% and 77% of all cells fell into the PrE cluster 0, whereas this cluster contained only between 35% and 42% of all cells in the *Med12* mutants (Fig. 6I). We then used the cell type annotation based on this clustering approach to ask how similar the changes in gene expression profiles were between wild-type and *Med12*-mutant cells upon differentiation towards either of the two lineages. We first focused on genes that had a log2 fold change ≥ 0.5 between pluripotency and differentiation in wild-type cells. The fold-changes of these genes in the mutant showed a unimodal distribution in all four conditions (up- and downregulation, Epi and PrE differentiation), indicating that *Med12* is not required for the regulation of specific gene modules during differentiation (Fig. 6J). This conclusion was supported by plotting the fold-change of all genes upon differentiation against each other for wild-type and mutant cells (Fig. 6 Supp 1 A, B). When comparing the top differentially expressed genes between wild type and mutant in pluripotency conditions as well as in the Epi and PrE clusters, we found that many of these genes were differentially expressed in all three states (Fig. 6 Supp 1C, Supp Table 6). This suggests that loss of *Med12* does not prevent differentiation, but rather results in gene expression changes that are shared between cell states.

Despite not regulating specific differentiation-associated gene modules, loss of *Med12* could still influence the efficiency of lineage separation. In the PCA plot in Fig. 6E, we noted that transcriptomes of Epi and PrE cells were separated more clearly in *Med12*-mutant compared to wild-type cultures. The Jaccard index is a quantitative measure for the separation of clusters in single cell sequencing data (Tang et al., 2021). We therefore computed the Jaccard index for clustering of 100 random subsets of each differentiated sample without integration (Materials and Methods). The average Jaccard index was higher in *Med12*-mutant samples compared to wild type, demonstrating that loss of *Med12* indeed leads to a better transcriptional separation of clusters (Fig. 6K). This could be a consequence of different transgene induction dynamics between genotypes, or result from a reduction of cellular plasticity upon loss of *Med12.* Consistent with differences in plasticity, wild-type cells, but not *Med12*-mutant cells, showed a long tail of the Jaccard index distribution indicating the presence of a population of cells that explore transcriptional space beyond the main clusters. As an alternative measure, we used VarID2 (Rosales-Alvarez et al., 2023) to test if biological noise levels were changed upon loss of *Med12*. This analysis revealed reduced noise levels in *Med12* mutants in all three differentiation states, with the strongest changes in pluripotency and in Epi cells (Fig. 6L). Taken together, these results indicate that loss of *Med12* results in

overall lower transcriptional output and decreased noise. These effects may result in reduced cellular plasticity during lineage transitions, which can enhance separation between lineages.

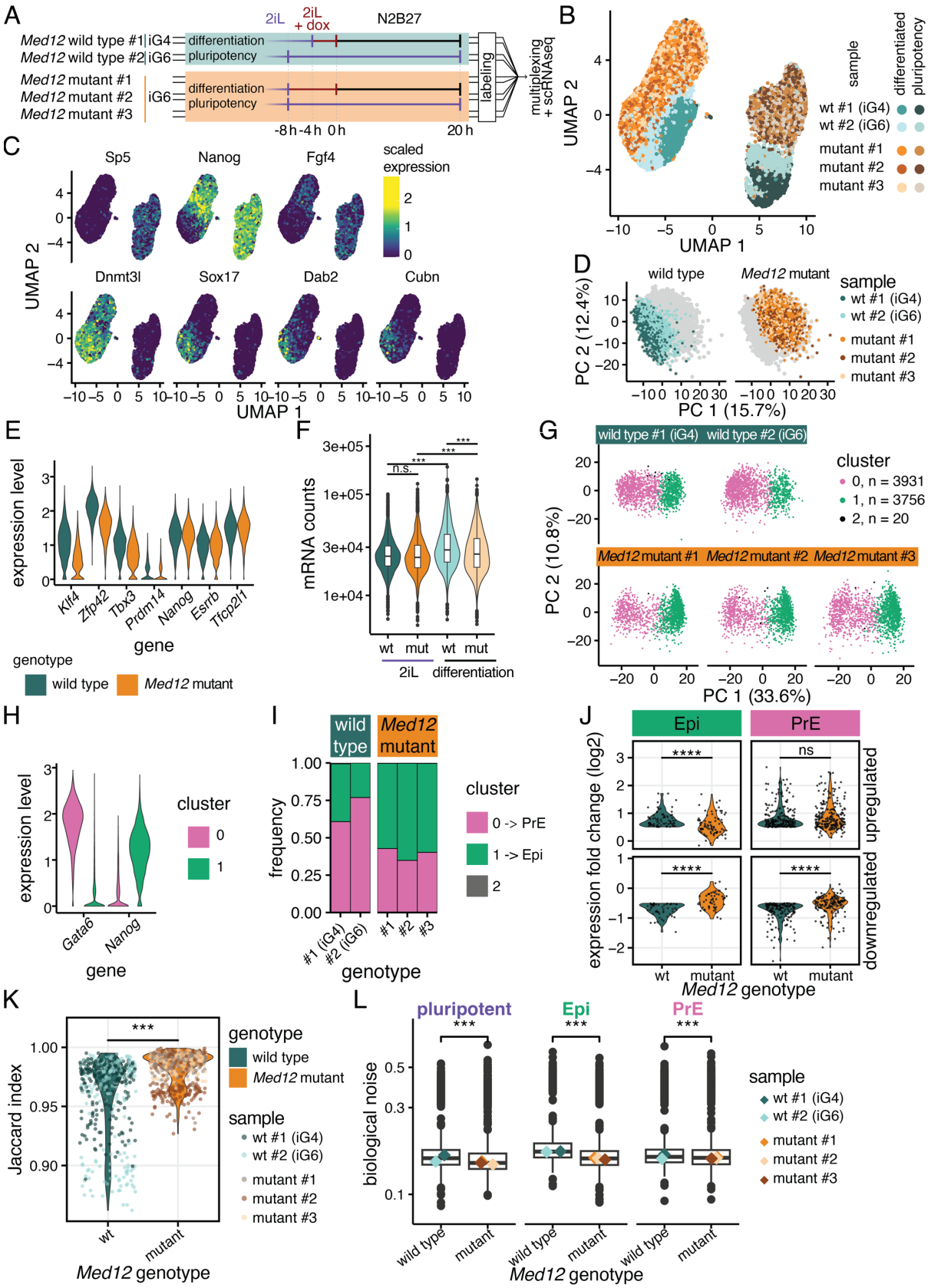

Fig. 6: Role of *Med12* in PrE differentiation.

A Schematic of the single cell RNA sequencing experiment to compare single cell transcriptional signatures between wild-type and *Med12*-mutant cells in pluripotency and upon PrE differentiation. Replicates were generated by including two *Med12* wild-type lines carrying inducible GATA4- or

GATA6-mCherry transgenes (iG4 and iG6), and three independent *Med12*-mutant cell lines derived from the GATA6-mCherry inducible line. Doxycycline induction was 4 h and 8 h in wild-type and *Med12*-mutant cells, respectively.

B UMAP plot of single cell transcriptomes from all 10 samples.

C Ln-scaled expression levels of selected marker genes projected onto the UMAP plot from (B).

D Principal component analysis of single cell transcriptomes from wild-type and *Med12*-mutant cells in pluripotency conditions.

E Ln-transformed expression levels of same naïve pluripotency marker genes as in Fig. 4C,D.

F Number of detected mRNAs per cell in wild-type and *Med12*-mutant cells. ns indicates $p \geq 0.05$, *** indicates $p \leq 0.001$, Bonferroni-adjusted Kolmogorov-Smirnov test.

G Principal component analysis and Louvain-clustering of single-cell transcriptomes from wild-type and *Med12*-mutant cells after differentiation.

H Ln-transformed expression levels of the PrE-marker gene *Gata6* and the Epi-marker gene *Nanog* in the differentiated samples split by cluster. Cluster 2 was excluded due to the small number of cells.

I Proportions of cell types, identified by clustering, in wild-type and *Med12*-mutant cells.

J Comparison of up- (top panels) and downregulated genes (bottom panels) in wild-type and *Med12*-mutant cells upon differentiation from pluripotency to Epi (left) or PrE (right). Shown are genes with a log2-change of expression > 0.5 in wild-type cells. ns indicates $p \geq 0.05$, **** indicates $p \leq 0.0001$, paired Wilcoxon signed rank test.

K Jaccard index to assess cluster stability of wild-type and *Med12*-mutant cells. ns indicates $p \geq 0.05$, *** indicates $p \leq 0.001$, Kolmogorov-Smirnov test.

For clarity, measurements from the two *Med12* wild-type and the three *Med12*-mutant lines were pooled in panels E, F, J, and for the violin plot and statistical test in K.

L Biological noise determined for each cell state (pluripotency, Epi and PrE) and genotype (*Med12* wild type and mutant) using VarID2 (Rosales-Alvarez et al., 2023). Medians for single clonal lines are indicated as diamond. **** indicates $p \leq 0.0001$, Wilcoxon signed rank test. Bar indicates median, boxes indicate 25^{th} and 75^{th} percentile.

Discussion

Here we use a *Spry4*$^{H2B\text{-}Venus}$ reporter to screen for regulators of developmental gene expression in pluripotent stem cells. This screen returned components of the FGF/ERK and the mTOR signaling systems that positively and negatively regulate reporter expression, respectively, as well as several members of the Mediator and Elongator complexes. Focusing on *Med12* we show that it cooperates with multiple signaling systems to regulate gene expression in pluripotent cells. Functional assays reveal that loss of *Med12* both reduces the ability to re-establish a naïve pluripotency gene expression program in colony forming assays, as well as the propensity to populate transition states in an epiblast-to-primitive endoderm differentiation paradigm. These phenotypes correlate with reduced noise in *Med12*-mutant cells. Together, these results suggest that *Med12* amplifies transcriptional changes in pluripotent cells, and thereby contributes to the maintenance of cellular plasticity during differentiation and lineage transitions.

Previous genome-wide screens have used retention of clonogenicity or the continued expression of pluripotency-associated reporter alleles in differentiation conditions as read-outs to identify regulators of pluripotency and lineage transitions (Betschinger et al., 2013; Kagey et al., 2010; M. Li et al., 2018; Villegas et al., 2019). In our study, the combination of a *Spry4*$^{H2B\text{-}Venus}$ allele with flow sorting constitutes a highly sensitive read-out that is focused on the activity of specific signaling systems in pluripotent cells, and reliably detects new regulators even if they have only small effect sizes. The screen's specificity shows in the strong representation of genes involved in the FGF/ERK signaling cascade, from genes that encode synthetases for FGF co-factors, over FGF receptors, to intracellular signaling genes. Surprisingly however, we did not find any sequence-specific transcription factors downstream of FGF/ERK signaling in our screen. This could be explained by the expression of multiple functionally redundant FGF/ERK signaling effectors in pluripotent cells, or through previously proposed transcription factor-independent regulation of RNA polymerase activity by ERK (Tee et al., 2014).

In addition to components of FGF and mTOR signaling systems, the screen returned several members of the SWI/SNF and the Mediator complexes. The core Mediator complex is thought to be required for the expression of most genes in eukaryotic genomes, but individual subunits have been suggested to regulate gene expression downstream of specific signaling systems such as the serum response network (Donner et al., 2010; Stevens et al., 2002), or Wnt (Rocha et al., 2010). However, when we tested this idea for *Med12*, we found that its loss did not phenocopy the effects of specific signaling perturbations. This finding suggests that previously reported functional connections, such as the link between *Med12* and Wnt signaling (Rocha et al., 2010), are strongly context-dependent.

Med12 is a critical component of the Mediator-associated CDK8-module. In contrast to pharmacological inhibition of CDK8 which has been reported to boost pluripotency similarly to ERK signaling inhibition (Lynch et al., 2020), we find that loss of *Med12* leads to reduced pluripotency. These opposing phenotypes indicate that MED12 has functions that are independent from the CDK8-module (Aranda-Orgilles et al., 2016). This would also explain why we did not detect any other CDK8-module components in our screen. Lynch et al. found that maintenance of pluripotency required the presence of CDK8, but absence of its kinase activity. Another possible explanation for the opposing phenotypes of CDK8 inhibition and *Med12* loss-of-function therefore is that MED12 participates in assembling kinase-inactive CDK8 complexes that support pluripotency.

Med12's function to maintain pluripotency reported in the present work is supported by earlier studies which found that MED12 and NANOG proteins interact, that MED12 and NANOG have similar DNA-binding profiles, and that MED12 promotes *Nanog* expression (Apostolou et al., 2013; Tutter et al., 2009). Several Mediator subunits, including *Med12*, have been identified in a screen for pluripotency maintenance that focused on transcription and chromatin regulators (Kagey et al., 2010). This study furthermore suggested that interactions between Mediator and cohesin contribute to genome folding and efficient enhancer-promoter interactions. When we probe *Med12* functions in lineage transitions, we find that *Med12*-mutant cells show decreased transcriptional plasticity, which manifests in a slower downregulation of pluripotency genes, a decreased ability to revert to naïve pluripotency in a colony-forming assay, and a reduced tendency to populate transition states in the binary decision between an epiblast and a primitive endoderm identity. We speculate that these cellular phenotypes are a reflection of a reduced ability of *Med12*-mutant cells to reconfigure the chromatin upon changing signaling environments. It is likely that the expression of individual genes is differentially sensitive to the loss of *Med12*. This may be the reason why expression from the *Sprouty4* locus, which is the most strongly upregulated gene upon acute FGF stimulation, shows a particularly high sensitivity to loss of *Med12*. In line with this idea, requirements of *Med12* for efficient induction are not exclusive to endogenous genes, but extend to exogenous transgenes such as the inducible GATA6-mCherry construct used to trigger primitive endoderm differentiation in our study. Surprisingly, such differential quantitative defects in the regulation of single genes upon loss of *Med12* do not lead to strong defects in acquiring early differentiated fates, such that transcriptomes of individual differentiated cells are not systematically different from each other in *Med12*-mutant and wild-type cells. This suggests that intracellular regulatory networks can buffer the composition of cellular transcriptomes against variable transcription efficiencies.

Acknowledgements

We thank Kristin Nowak for generating *Fgf4*-mutant E14tg2a mESC lines, members of the Imig lab for help with lentivirus production, and the protein chemistry facility of the MPI Dortmund for supply of LIF and enzymes for molecular biology. Michelle Marten provided technical and organizational support for tissue culture and flow sorting throughout the project. We thank members of the Schröter lab, the Department of Systemic Cell Biology, Jochen Imig and Cristina Pina for critical discussions and feedback on earlier versions of the manuscript. This work was funded by the Deutsche Forschungsgemeinschaft (project no. 441798639), the Volkswagen Foundation (project no. A130140), and the Max Planck Society.

Declaration of interest

The authors declare that they have no conflict of interest.

Materials and Methods

Cell culture

Routine culture of mESCs was performed at 37 °C with 5% CO_2 in either serum + LIF medium (ESL, composed of GMEM with 10% fetal bovine serum (FBS), 2 mM GlutaMAX, 1 mM sodium pyruvate, 0.1 mM b-mercaptoethanol and 10 ng/mL LIF), on 0.1% gelatine coated dishes, or in 2i + LIF medium on fibronectin coated dishes. 2i + LIF is N2B27 supplemented with 1 µM PD0325901 (SelleckChem), 3 µM CHIR99201 (Tocris) and 10 ng/ml LIF (protein chemistry facility, MPI Dortmund). N2B27 was prepared as a 1:1 mixture of DMEM/F12 and Neuropan Basal Medium (both from PAN Biotech), supplemented with 1X N2 and 1X B27 supplements, 1X L-Glutamax, 0.0025% BSA, and 0.2 mM ß-mercaptoethanol (all from ThermoFisher). *Fgf4*-mutant cell lines were cultured in 2i + LIF supplemented with 10% FBS. Cells were passaged every two to three days, and detached with trypsin (PAN Biotech) or Accutase (Sigma-Aldrich).

Cell lines

All cell lines generated in this study were derived from the E14tg2a wild-type line (Hooper et al., 1987). The GATA4-mCherry inducible line used for single cell RNA sequencing has been described previously (Raina et al., 2021). The *Spry4*$^{H2B\text{-}Venus/+}$-reporter line was generated with a previously described targeting construct (Morgani et al., 2018) using lipofectamine 2000 according manufacturer's instructions (Thermo Fisher Scientific). Correctly targeted clones were identified via long-range PCR as described in (Morgani et al., 2018). GATA6-mCherry inducible lines were established as described for GATA4-mCherry inducible lines in (Raina et al., 2021), but replacing the *Gata4* with a *Gata6* coding sequence in the PiggyBac vector for inducible gene expression. We established multiple clonal lines and tested them for GATA6-mCherry induction levels upon dox-treatment by flow cytometry. Three independent clones with induction levels similar or slightly higher than the previously established GATA4-mCherry inducible lines were selected for the experiment shown in Fig. 5D, and a single clonal line was chosen for all other experiments. Newly generated *Spry4*$^{H2B\text{-}Venus/+}$-reporter and GATA6-mCherry inducible cell lines were checked for karyotypic abnormalities. To label nuclei for time lapse imaging cells were transfected with pCX-H2B-Cerulean- IRES-puro (Schumacher et al., 2023). Cell lines carrying PiggyBac transgenes were kept under appropriate selection to prevent transgene repression over passaging.

sgRNA cloning and generation of single-gene mutants

For mutagenesis of individual genes via CRISPR/Cas9, gene targeting sgRNAs (Supp Table 7) were cloned into pX459 (Addgene plasmid #48139) using BbsI (NEB) overhangs following Ran et al., 2013 (Ran et al., 2013). Clonal mutant lines were generated using a combination of sgRNAs with targeting sequences 100 to 200 bp apart in the genome. Single sgRNAs were used when generating polyclonal lines. For validation experiments of the CRISPR screen (Figs 1 and 2), we selected the most enriched sgRNA in sorted cells. A total of 1 µg of sgRNA containing px459 vectors was mixed with a final concentration of 0.04 µg/ml Lipofectamine 2000 (Thermo Fisher Scientific) in Opti-MEM (Gibco) according to the manufacturer's protocol. For the generation of clonal lines, cells were seeded at clonal density into 10 cm dishes after transfection, for polyclonal experiments approximately 50k cells/cm^2 were seeded. To enrich for successfully transfected cells, selection with 1.5 µg/ml puromycin was started 24 h after transfection for 48 h. To establish clonal lines, single-cell derived colonies were picked 4 to 6 d after transfection and expanded. For molecular characterization of genetic lesions, genomic DNA was purified with Terra™ PCR Direct Genotyping Kit (Takara), followed by PCR amplification and Sanger sequencing of specific genomic regions encompassing the target site.

Genome-wide CRISPR Screen

To generate stably CAS9-expressing *Spry4*$^{H2B\text{-}Venus/+}$ reporter cells, cells were transduced with lentiCas9-Blast lentiviral particles (Addgene #52962-LV) at a multiplicity of infection of approximately 0.1. Transduction was performed with attached cells, 20 h after seeding at 20 000 cells/cm^2, in presence of 5 µg/ml Polybrene in ESL. Continuous blasticidin (15 µg/ml, Gibco) selection was started 24 h after transduction. Lentiviral particles of the genome-wide gRNA library Brie (Addgene #73633) were generated according to standard protocols (Doench et al., 2016). For library transduction, 150 * 10^6 CAS9-expressing *Spry4*$^{H2B\text{-}Venus/+}$ reporter cells were detached and mixed with the virus library in ESL with 5 µg/ml Polybrene. The following day, the same number of cells was reseeded and put under selection with puromycin (1.5 µg/ml, Sigma-Aldrich). Comparing cell counts with and without selection indicated a transduction efficiency of 25%, resulting in a >400-fold coverage of transduced cells per gRNA. In all subsequent steps, at least 31 * 10^6 cells were processed to maintain gRNA coverage.
To identify gRNAs enriched in cell populations with high and low *Spry*4:H2B-Venus expression, at least 0.5 * 10^6 cells with the lowest or highest 1% of *Spry*4:H2B-Venus fluorescence, or 3 * 10^6 cells with the lowest or highest 5% of *Spry*4:H2B-Venus fluorescence were FAC sorted and their DNA isolated by column-based genomic DNA purification (Monarch

Genomic DNA Purification Kit, NEB). For reference, the genomic DNA of 31 * 10^6 non-sorted control cells was purified in parallel. The integrated gRNA was PCR amplified using Pfu polymerase (prepared in house) with a sample specific, sequencing adapter and index containing primers (Supp Table 7; Carlini et al., 2021) using the complete purified genomic DNA as template. PCR-samples were purified with the SPRIselect reagent (Beckman Coulter) with double-sided size selection. Briefly, 0.5x SPRIselect was added to each sample, incubated for 5 min at RT and the SPRIselect removed with a magnet. This supernatant was again mixed with 1.2x SPRIselect, incubated and then discarded. After washing the beads, the DNA library was eluted from the beads and used for sequencing.
Paired-End Illumina Sequencing with a read length of 150 bp pairs was performed with at least 10 * 10^6 reads per sorted sample and 30 * 10^6 reads for the unsorted library controls. The raw reads were trimmed using Cutadapt (Martin, 2011) to remove the vector binding sequence. The reads were mapped to individual gRNAs, counted using *norm-method total* and statistically tested on the targeted gene levels using *gene-lfc-method alphamean* with Mageck (W. Li et al., 2014). Hits were selected based on the false discovery rate.

Immunostaining

Immunostaining was performed as previously described (Schröter et al., 2015), Briefly, cells were washed with PBS containing Calcium and Magnesium, followed by fixation with 4% paraformaldehyde (Histofix, Sigma-Aldrich) for 15 min. Cells were permeabilized and blocked by rinsing and washing three times with PBS with 0.1% Triton X-100 and 1.0% bovine serum albumin (PBT-BSA). Primary antibodies (Anti-mouse NANOG (Affymetrix eBioscience, Cat.:14-5761), Anti-SOX17 (R&D systems, Cat.: AF1924)) were diluted 1:200 in PBT-BSA and incubated with the cells overnight at 4 °C. The next day, cells were washed in PBT-BSA and incubated with Alexa Fluor-conjugated secondary antibodies at 4 µg/ml (Invitrogen/Life Technologies) and Hoechst 33342 at 1 µg/ml (Invitrogen) in PBT-BSA in the dark for 2 h. Finally, samples were rinsed and washed with PBS and imaged in a mounting medium consisting of 80% glycerol, 16% PBS and 4% n-propyl-gallate.

Immunoblotting

For western blot analysis of MED12 and ppERK, cells were washed twice with ice-cold PBS, supplemented with 1 mM activated orthovanadate in case of ppERK detection. Cells were mechanically detached in lysis buffer, based on commercially available lysis buffer (Cell Signaling) supplemented with benzonase (Sigma-Aldrich), cOmplete EDTA-free protease inhibitor cocktail (Roche), phosphate inhibitors P1 and P2 (Sigma). The lysates were snap

frozen in liquid nitrogen twice and centrifuged. Protein concentration in the supernatant was measured with a micro BCA assay (Thermo Scientific). For western analysis, 20 µg of protein per sample were denatured by adding 5x Laemelli buffer and incubation at 95 °C for 5 min. The SDS-PAGE was run in 1x MOPS buffer (ThermoFisher) with 5 mM sodium-bisulfate and immediately transferred onto methanol-activated PVDF membranes. Transfer was performed in transfer buffer (12mM Tris-Base, 96mM Glycine, 20% methanol) at 40 V for 1.5 h in a NuPage transfer system (ThermoFisher). Membranes were blocked at RT for 1 h in Intercept blocking buffer (LI-COR), which was also used for the dilution and incubation with the primary antibodies anti-Tubulin 1:10000 (T6074, Sigma), anti-pERK1/2 1:1000 (4370S, Cell Signaling), anti-total ERK1/2 1:1000 (ab36991, Abcam) or anti-Med12 (1:250, A300-774A, Bethyl Laboratories). Appropriate secondary antibodies (IRdyes, LI-COR) were used at a dilution of 1:5000. Blots were imaged on an Odyssey CLx (LI-COR). Quantification of ppERK bands was performed using the gel quantification tool in Fiji, using the combined intensities of ERK1 and ERK2 bands, and normalizing ppERK by total ERK signals.

Imaging

Tilescans of immunostainings were imaged with a Leica SP8 confocal microscope (Leica Microsystems) with a 63x 1.4 NA oil immersion objective. Images were analyzed in Fiji (Schindelin et al., 2013). For segmentation, StarDist 2D (Schmidt et al., 2018) was used using the versatile (fluorescent nuclei) model and default post processing parameters. Mean fluorescence intensity was measured in segmented cells in all acquired channels. Cells with a nuclear area smaller than 40 μm^2 were filtered out. To determine fluorescence intensity threshold values for the classification of cell types, we manually selected thresholds that best bisected the bimodal expression profiles of the lineage markers. The same thresholds were applied to different samples in a single experiment.

Images of live *Spry4*$^{H2B\text{-}Venus/+}$-reporter cells were acquired with an Olympus IX81 widefield microscope, equipped with a stage top incubator (ibidi), pE4000 illumination (CoolLED), ORCA-Quest qCMOS camera (Hamamatsu) with a 63x 1.35 NA oil immersion objective. Hardware was controlled by Olympus CellSens Software. Time lapse imaging was performed with a 40x 0.9 NA objective on an Olympus IX81 widefield microscope, equipped with an LED-based illumination system (pE4000, CoolLED) and an iXon 888 EM-CCD camera (Andor). MicroManager (Edelstein et al., 2010) was used to control the hardware. Images were taken every 10 min. Tracking was performed with the manual tracking function in Trackmate v7 (Ershov et al., 2022) and fluorescence intensity was measured as the mean intensity in a spot with a 4 µm radius within the nucleus. In R, tracks were smoothed with a rolling average over

7 frames. For ROC analysis the R package pROC (Robin et al., 2011) was applied and the optimal threshold was defined by the Youden's J statistic (Youden, 1950).

Flow cytometry

Analysis of *Spry4*:H2B-Venus reporter expression in live or fixed cells was performed on a LSRII flow cytometer (BD Biosciences). Cell sorting and analysis of GATA6-mCherry expression was carried out using a FACS Aria Fusion (BD Biosciences). Primary data analysis including gating single cells based on SSC and FSC was done with FlowJo version 9 (BD Biosciences).

Clonogenicity Assay

Clonogenicity assays were performed according to (Kalkan et al., 2017). Briefly, $1 * 10^4$ cells/cm^2 were seeded in 2i + LIF for 24 h, followed by differentiation in N2B27 for 48 h. Control wells for each parental cell line were kept in 2i + LIF. Cells were then detached with Accutase to single cells, and 500 cells were reseeded into 6-well plates with 2i + LIF + 10% FBS. 10% FBS were included to support survival of *Fgf4*-mutant cells.
After 5 d, the colonies formed were fixed and stained with an alkaline phosphatase assay kit (Sigma-Aldrich) to distinguish pluripotent and differentiated colonies. Tile scans of the wells were acquired with an Olympus IX81 widefield microscope with a 4x 0.16 NA objective. We applied background subtraction, gaussian blurring, Otsu-thresholding, and conversion of images to a binary mask in ImageJ, and then used the *AnalyzeParticles* function to set thresholds for size and circularity and to determine the number of colonies. Colony numbers were normalized to the number of colonies obtained in the control.

Bulk RNA sequencing

For bulk RNA sequencing, cells were seeded at a density between 3.5 and $5.5 * 10^4$ cells/cm^2 in 2i or N2B27 + Chiron + LIF, followed by stimulation under indicated conditions. Replicates were obtained either from independent biological experiments (Fig. 3 A, B) or from both independent biological experiments and independent *Med12*-mutant lines (Fig. 3F, G). RNA isolation was performed with TRIzol (ambion) according to the manufacturer's instructions. Sequencing libraries were prepared on polyA-enriched RNAs, followed by paired-end sequencing at a read-length of 150 bp and depth of approximately $30 * 10^6$ reads per sample. Strand-specific libraries were generated only for the FGF-titration experiment (Fig. 1 Supp 1) and the differentiation of the *Med12* wild-type and mutant cells (Fig. 3A, B). Raw reads were

mapped to the mouse genome (GRCm39, release 108 (both *Med12* mutant experiments) or release 97 (FGF titration experiment) with hisat2 (v2.1.0; Kim et al., 2019). SeqMonk was used to quantify counts per gene, either as TPM or as raw counts as input for downstream DESeq2 analysis (Love et al., 2014) for identification of differentially expressed genes.

Differentiation delay in Med12 mutants was estimated according to (Lackner et al., 2021). We first determined the expression change of the naïve marker genes *Nanog*, *Esrrb*, *Tbx3*, *Tfcp2l1*, *Klf4*, *Prdm14* and *Zfp4* in *Med12*-mutant and wild-type cells, and then plotted the Euclidean distance of this expression change to that of the time-resolved dataset from Lackner et al., 2021.

Signaling footprint analysis in *Med12* mutants was performed similarly to Lacker et al., 2021. This study defined a specific set of target genes for each pluripotency associated signaling system based on gene expression changes in knockouts of signaling genes. A signaling footprint for a knockout line can then be determined from the difference in the expression of pathway footprint genes to the wild-type line after 24 h of differentiation. Measures for the signaling footprint are the Spearman correlation between each knockout line and the respective pathway defining knockout, and the ratio between the sum of expression fold changes between a knockout line and the respective pathway defining knockout, defined as pathway activity. To compare the *Med12* mutant data from this study, the wild type conditions were used for batch correction.

Cell multiplexing and scRNA sequencing

Cells for scRNAseq were seeded at a density of 3.5 * 10^4 cells/cm^2 in 6-well plates in 2i + LIF and grown overnight. The next morning, induction in 2i + LIF + dox was first started in the mutant clones, and 4 h later in the wild-type lines. After 8h and 4 h, respectively, induction was stopped by washing once with N2B27, followed by 20 h of differentiation in N2B27. Controls for each cell line were continuously kept in 2i + LIF. For sequencing, cells were washed three times with PBS and detached with Accutase. Accutase was removed by centrifugation and 1 * 10^6 cells per sample were resuspended in PBS + 0.04 % BSA and immediately used for multiplexing labeling following the protocol of 10x Genomics for samples with a viability above 80 % (Cell Multiplexing Oligo Labeling for Single Cell RNA Sequencing Protocols with Feature Barcode technology, CG000391). Briefly, cells were spun down once again, resuspended with individual cell multiplexing oligos (CMO no. 301 to 310) and incubated for 5 min at RT. Cells were washed twice with PBS + 1 % BSA and passed through a cell strainer (FALCON, mesh size 35 µm). A total of 1.2 * 10^5 single cells from all samples were pooled at equal ratios, and 4 * 10^4 were used for droplet generation, corresponding to a target number of 2.4 * 10^4 cell-containing droplets. Droplet generation, lysis, mRNA and cell barcode capture, and generation

of both the gene expression library as well as the cell multiplexing library was performed following the instructions by 10x genomics (Chromium Next GEM Single Cell 3' Reagent Kits v3.1 (Dual Index) with Feature Barcode technology for Cell Multiplexing, CG000388). Specifically, we chose 11 PCR cycles for cDNA amplification and 10 cycles for the sample index PCR. Concentration and insert size distribution for both the gene expression library and the cell multiplexing library were determined with a BioAnalyzer High Sensitivity DNA Assay (Agilent). Sequencing was performed on a NovaSeq 6000 on multiple flowcells with a paired-end 150 bp configuration. In total $1.2 * 10^9$ and $2.3 * 10^8$ read pairs were obtained for the gene expression and multiplexing library, respectively.

Demultiplexing to the individual samples, based on the cell multiplexing barcode and alignment to the mouse genome mm10 (GENCODE vM23/Ensembl 98, obtained from 10x Genomics) was performed with CellRanger (version 7.1.0, 10x Genomics). Downstream analysis was performed in R with Seurat v5 (Hao et al., 2023). We first filtered cells by removing barcodes with ≤ 2500 detected genes and ≥15 % of reads aligned to mitochondrial genes, retaining between 1100 and 1700 cells per sample with median mRNA counts per cell between 23233 and 27890 in the different samples. mRNA counts for each gene were normalized by dividing its counts by the total number of counts per cell, multiplied by 10000. Log1p transformation was applied before plotting expression data as violin plots. For downstream analysis and representation of gene expression as heatmaps, centering counts for each feature and scaling to its standard deviation was applied. Principal component analysis was performed on the 2000 most variable features in the relevant subset of cells. The resolution of the Louvain clustering algorithm was set to 0.05 when clustering multiple samples. In case of Jaccard-Index estimation the clustering resolution was set to 0.15 and the clustering was performed on each sample separately. 100-fold repetition of this clustering approach with a random subset of the data with 70 % of the cells allowed the calculation of a Jaccard-index, as previously described (Tang et al., 2021). For annotation of the Epi- and PrE-fate, the cells of the differentiated samples were integrated with Seurat integration based on the *rpca* reduction. Differentially expressed genes between cell states and genotypes were identified with the *FindMarkers* function in Seurat with a minimal expression difference in the log1p transformed expression values of 0.5. Biological noise was quantitated and distinguished from modeled technical noise in local neighborhoods of each cell with VarID2 (Rosales-Alvarez et al., 2023).

Data and code availability

Sequencing data from this paper has been deposited at GEO with accession number GSE253609. All code used for analysis and visualization, together with a list of the R packages used, is available from the authors upon request.

Bibliography

Apostolou, E., Ferrari, F., Walsh, R. M., Bar-Nur, O., Stadtfeld, M., Cheloufi, S., Stuart, H. T., Polo, J. M., Ohsumi, T. K., Borowsky, M. L., Kharchenko, P. V., Park, P. J., & Hochedlinger, K. (2013). Genome-wide chromatin interactions of the nanog locus in pluripotency, differentiation, and reprogramming. *Cell Stem Cell*, *12*(6), 699–712. https://doi.org/10.1016/j.stem.2013.04.013

Aranda-Orgilles, B., Saldaña-Meyer, R., Wang, E., Trompouki, E., Fassl, A., Lau, S., Mullenders, J., Rocha, P. P., Raviram, R., Guillamot, M., Sánchez-Díaz, M., Wang, K., Kayembe, C., Zhang, N., Amoasii, L., Choudhuri, A., Skok, J. A., Schober, M., Reinberg, D., … Aifantis, I. (2016). MED12 Regulates HSC-Specific Enhancers Independently of Mediator Kinase Activity to Control Hematopoiesis. *Cell Stem Cell*, *19*(6), 784–799. https://doi.org/10.1016/j.stem.2016.08.004

Athanasouli, P., Balli, M., De Jaime-Soguero, A., Boel, A., Papanikolaou, S., van der Veer, B. K., Janiszewski, A., Vanhessche, T., Francis, A., El Laithy, Y., Nigro, A. Lo, Aulicino, F., Koh, K. P., Pasque, V., Cosma, M. P., Verfaillie, C., Zwijsen, A., Heindryckx, B., Nikolaou, C., & Lluis, F. (2023). The Wnt/TCF7L1 transcriptional repressor axis drives primitive endoderm formation by antagonizing naive and formative pluripotency. *Nature Communications*, *14*(1), 1–19. https://doi.org/10.1038/s41467-023-36914-1

Betschinger, J., Nichols, J., Dietmann, S., Corrin, P. D., Paddison, P. J., & Smith, A. (2013). Exit from pluripotency is gated by intracellular redistribution of the bHLH transcription factor Tfe3. *Cell*, *153*(2), 335–347. https://doi.org/10.1016/j.cell.2013.03.012

Carlini, V., Gretarsson, K. H., & Hackett, J. A. (2021). Genome-scale CRISPR screening for regulators of cell fate transitions. In *Methods in Molecular Biology* (Vol. 2214, pp. 91–108). Humana Press Inc. https://doi.org/10.1007/978-1-0716-0958-3_7

Chazaud, C., & Yamanaka, Y. (2016). Lineage specification in the mouse preimplantation embryo. *Development (Cambridge)*, *143*(7), 1063–1074. https://doi.org/10.1242/DEV.128314

Doench, J. G., Fusi, N., Sullender, M., Hegde, M., Vaimberg, E. W., Donovan, K. F., Smith, I., Tothova, Z., Wilen, C., Orchard, R., Virgin, H. W., Listgarten, J., & Root, D. E. (2016). Optimized sgRNA design to maximize activity and minimize off-target effects of CRISPR-Cas9. *Nature Biotechnology*, *34*(2), 184–191. https://doi.org/10.1038/nbt.3437

Donner, A. J., Ebmeier, C. C., Taatjes, D. J., & Espinosa, J. M. (2010). CDK8 is a positive regulator of transcriptional elongation within the serum response network. *Nature Structural and Molecular Biology*, *17*(2), 194–201. https://doi.org/10.1038/nsmb.1752

Edelstein, A., Amodaj, N., Hoover, K., Vale, R., & Stuurman, N. (2010). Computer control of microscopes using μManager. *Current Protocols in Molecular Biology*, *Chapter 14*(SUPPL. 92). https://doi.org/10.1002/0471142727.MB1420S92

Ershov, D., Phan, M. S., Pylvänäinen, J. W., Rigaud, S. U., Le Blanc, L., Charles-Orszag, A., Conway, J. R. W., Laine, R. F., Roy, N. H., Bonazzi, D., Duménil, G., Jacquemet, G., & Tinevez, J. Y. (2022). TrackMate 7: integrating state-of-the-art segmentation algorithms into tracking pipelines. *Nature Methods*, *19*(7), 829–832. https://doi.org/10.1038/s41592-022-01507-1

Fawcett, T. (2006). An introduction to ROC analysis. *Pattern Recognition Letters*, *27*(8), 861–874. https://doi.org/10.1016/J.PATREC.2005.10.010

Fujikura, J., Yamato, E., Yonemura, S., Hosoda, K., Masui, S., Nakao, K., Miyazaki, J. I., & Niwa, H. (2002). Differentiation of embryonic stem cells is induced by GATA factors. *Genes & Development*, *16*(7), 784–789. https://doi.org/10.1101/GAD.968802

Hanna, R. E., & Doench, J. G. (2020). Design and analysis of CRISPR–Cas experiments. In *Nature Biotechnology* (Vol. 38, Issue 7, pp. 813–823). Nature Research. https://doi.org/10.1038/s41587-020-0490-7

Hao, Y., Stuart, T., Kowalski, M. H., Choudhary, S., Hoffman, P., Hartman, A., Srivastava, A., Molla, G., Madad, S., Fernandez-Granda, C., & Satija, R. (2023). Dictionary learning for integrative, multimodal and scalable single-cell analysis. *Nature Biotechnology*, 1–12. https://doi.org/10.1038/s41587-023-01767-y

Hooper, M., Hardy, K., Handyside, A., Hunter, S., & Monk, M. (1987). HPRT-deficient (Lesch-Nyhan) mouse embryos derived from germline colonization by cultured cells. *Nature*, *326*(6110), 292–295. https://doi.org/10.1038/326292A0

Kagey, M. H., Newman, J. J., Bilodeau, S., Zhan, Y., Orlando, D. A., Van Berkum, N. L., Ebmeier, C. C., Goossens, J., Rahl, P. B., Levine, S. S., Taatjes, D. J., Dekker, J., & Young, R. A. (2010). Mediator and cohesin connect gene expression and chromatin architecture. *Nature*, *467*(7314), 430–435. https://doi.org/10.1038/nature09380

Kalkan, T., Bornelöv, S., Mulas, C., Diamanti, E., Lohoff, T., Ralser, M., Middelkamp, S., Lombard, P., Nichols, J., & Smith, A. (2019). Complementary Activity of ETV5, RBPJ, and TCF3 Drives Formative Transition from Naive Pluripotency. *Cell Stem Cell*, *24*(5), 785-801.e7. https://doi.org/10.1016/j.stem.2019.03.017

Kalkan, T., Olova, N., Roode, M., Mulas, C., Lee, H. J., Nett, I., Marks, H., Walker, R., Stunnenberg, H. G., Lilley, K. S., Nichols, J., Reik, W., Bertone, P., & Smith, A. (2017). Tracking the embryonic stem cell transition from ground state pluripotency. *Development (Cambridge)*, *144*(7), 1221–1234. https://doi.org/10.1242/dev.142711

Kalkan, T., & Smith, A. (2014). Mapping the route from naive pluripotency to lineage specification. *Philosophical Transactions of the Royal Society B: Biological Sciences*, *369*(1657). https://doi.org/10.1098/RSTB.2013.0540

Kang, M., Piliszek, A., Artus, J., & Hadjantonakis, A. K. (2013). FGF4 is required for lineage restriction and salt-and-pepper distribution of primitive endoderm factors but not their initial expression in the mouse. *Development (Cambridge)*, *140*(2), 267–279. https://doi.org/10.1242/DEV.084996

Kim, D., Paggi, J. M., Park, C., Bennett, C., & Salzberg, S. L. (2019). Graph-based genome alignment and genotyping with HISAT2 and HISAT-genotype. *Nature Biotechnology*, *37*(8), 907–915. https://doi.org/10.1038/S41587-019-0201-4

Knuesel, M. T., Meyer, K. D., Donner, A. J., Espinosa, J. M., & Taatjes, D. J. (2009). The human CDK8 subcomplex is a histone kinase that requires Med12 for activity and can function independently of mediator. *Molecular and Cellular Biology*, *29*(3), 650–661. https://doi.org/10.1128/MCB.00993-08

Lackner, A., Sehlke, R., Garmhausen, M., Giuseppe Stirparo, G., Huth, M., Titz-Teixeira, F., Lelij, P., Ramesmayer, J., Thomas, H. F., Ralser, M., Santini, L., Galimberti, E., Sarov, M., Stewart, A. F., Smith, A., Beyer, A., & Leeb, M. (2021). Cooperative genetic networks drive embryonic stem cell transition from naïve to formative pluripotency. *The EMBO Journal*, *40*(8). https://doi.org/10.15252/embj.2020105776

Li, M., Yu, J. S. L., Tilgner, K., Ong, S. H., Koike-Yusa, H., & Yusa, K. (2018). Genome-wide CRISPR-KO Screen Uncovers mTORC1-Mediated Gsk3 Regulation in Naive Pluripotency Maintenance and Dissolution. *Cell Reports*, *24*(2), 489–502. https://doi.org/10.1016/j.celrep.2018.06.027

Li, W., Xu, H., Xiao, T., Cong, L., Love, M. I., Zhang, F., Irizarry, R. A., Liu, J. S., Brown, M., & Liu, X. S. (2014). MAGeCK enables robust identification of essential genes from genome-scale CRISPR/Cas9 knockout screens. *Genome Biology*, *15*(12), 554. https://doi.org/10.1186/s13059-014-0554-4

Love, M. I., Huber, W., & Anders, S. (2014). Moderated estimation of fold change and dispersion for RNA-seq data with DESeq2. *Genome Biology*, *15*(12), 1–21. https://doi.org/10.1186/s13059-014-0550-8

Luyties, O., & Taatjes, D. J. (2022). The Mediator kinase module: an interface between cell signaling and transcription. *Trends in Biochemical Sciences*, *47*(4), 314–327. https://doi.org/10.1016/j.tibs.2022.01.002

Lynch, C. J., Bernad, R., Martínez-Val, A., Shahbazi, M. N., Nóbrega-Pereira, S., Calvo, I., Blanco-Aparicio, C., Tarantino, C., Garreta, E., Richart-Ginés, L., Alcazar, N., Graña-Castro, O., Gómez-Lopez, G., Aksoy, I., Muñoz-Martín, M., Martinez, S., Ortega, S., Prieto, S., Simboeck, E., … Serrano, M. (2020). Global hyperactivation of enhancers stabilizes human and mouse naive pluripotency through inhibition of CDK8/19 Mediator kinases. *Nature Cell Biology*, *22*(10), 1223–1238. https://doi.org/10.1038/s41556-020-0573-1

Martin, M. (2011). Cutadapt removes adapter sequences from high-throughput sequencing reads. *EMBnet.Journal*, *17*(1), 10–12. https://doi.org/10.14806/EJ.17.1.200

Morgani, S. M., & Brickman, J. M. (2015). LIF supports primitive endoderm expansion during pre-implantation development. *Development (Cambridge)*, *142*(20), 3488–3499. https://doi.org/10.1242/DEV.125021

Morgani, S. M., Saiz, N., Garg, V., Raina, D., Simon, C. S., Kang, M., Arias, A. M., Nichols, J., Schröter, C., & Hadjantonakis, A. K. (2018). A Sprouty4 reporter to monitor FGF/ERK signaling activity in ESCs and mice. *Developmental Biology*, *441*(1), 104–126. https://doi.org/10.1016/j.ydbio.2018.06.017

Neagu, A., van Genderen, E., Escudero, I., Verwegen, L., Kurek, D., Lehmann, J., Stel, J., Dirks, R. A. M., van Mierlo, G., Maas, A., Eleveld, C., Ge, Y., den Dekker, A. T., Brouwer, R. W. W., van IJcken, W. F. J., Modic, M., Drukker, M., Jansen, J. H., Rivron, N. C., … ten Berge, D. (2020). In vitro capture and characterization of embryonic rosette-stage pluripotency between naive and primed states. *Nature Cell Biology*, *22*(5), 534–545. https://doi.org/10.1038/S41556-020-0508-X

Nichols, J., Silva, J., Roode, M., & Smith, A. (2009). Suppression of Erk signalling promotes ground state pluripotency in the mouse embryo. *Development (Cambridge)*, *136*(19), 3215–3222. https://doi.org/10.1242/dev.038893

Nichols, J., & Smith, A. (2009). Naive and Primed Pluripotent States. In *Cell Stem Cell* (Vol. 4, Issue 6, pp. 487–492). https://doi.org/10.1016/j.stem.2009.05.015

Ornitz, D. M., & Itoh, N. (2015). The fibroblast growth factor signaling pathway. *Wiley Interdisciplinary Reviews: Developmental Biology*, *4*(3), 215–266. https://doi.org/10.1002/wdev.176

Park, M. J., Shen, H., Spaeth, J. M., Tolvanen, J. H., Failor, C., Knudtson, J. F., McLaughlin, J., Halder, S. K., Yang, Q., Bulun, S. E., Al-Hendy, A., Schenken, R. S., Aaltonen, L. A., & Boyer, T. G. (2018). Oncogenic exon 2 mutations in Mediator subunit MED12 disrupt allosteric activation of cyclin C-CDK8/19. *The Journal of Biological Chemistry*, *293*(13), 4870–4882. https://doi.org/10.1074/JBC.RA118.001725

Raina, D., Bahadori, A., Stanoev, A., Protzek, M., Koseska, A., & Schröter, C. (2021). Cell-cell communication through FGF4 generates and maintains robust proportions of

differentiated cell types in embryonic stem cells. *Development (Cambridge)*, *148*(21). https://doi.org/10.1242/DEV.199926

Ran, F. A., Hsu, P. D., Wright, J., Agarwala, V., Scott, D. A., & Zhang, F. (2013). Genome engineering using the CRISPR-Cas9 system. *Nature Protocols*, *8*(11), 2281–2308. https://doi.org/10.1038/NPROT.2013.143

Robin, X., Turck, N., Hainard, A., Tiberti, N., Lisacek, F., Sanchez, J. C., & Müller, M. (2011). pROC: An open-source package for R and S+ to analyze and compare ROC curves. *BMC Bioinformatics*, *12*(1), 1–8. https://doi.org/https://doi.org/10.1186/1471-2105-12-77

Rocha, P. P., Scholze, M., Bleiß, W., & Schrewe, H. (2010). Med12 is essential for early mouse development and for canonical Wnt and Wnt/PCP signaling. *Development (Cambridge)*, *137*(16), 2723–2731. https://doi.org/10.1242/dev.053660

Rosales-Alvarez, R. E., Rettkowski, J., Herman, J. S., Dumbović, G., Cabezas-Wallscheid, N., & Grün, D. (2023). VarID2 quantifies gene expression noise dynamics and unveils functional heterogeneity of ageing hematopoietic stem cells. *Genome Biology*, *24*(1). https://doi.org/10.1186/s13059-023-02974-1

Schindelin, J., Arganda-carreras, I., Frise, E., Kaynig, V., Pietzsch, T., Preibisch, S., Rueden, C., Saalfeld, S., Schmid, B., Tinevez, J., White, D. J., Hartenstein, V., Tomancak, P., & Cardona, A. (2013). Fiji - an Open Source platform for biological image analysis. *Nature Methods*, *9*(7). https://doi.org/10.1038/nmeth.2019.Fiji

Schmidt, U., Weigert, M., Broaddus, C., & Myers, G. (2018). Cell detection with star-convex polygons. *Lecture Notes in Computer Science*, *11071 LNCS*, 265–273. https://doi.org/https://doi.org/10.1007/978-3-030-00934-2_30

Schröter, C., Rué, P., Mackenzie, J. P., & Arias, A. M. (2015). FGF/MAPK signaling sets the switching threshold of a bistable circuit controlling cell fate decisions in embryonic stem cells. *Development (Cambridge)*, *142*(24), 4205–4216. https://doi.org/10.1242/DEV.127530/-/DC1

Schumacher, S., Fernkorn, M., Marten, M., Kim, Y. S., Bedzhov, I., & Schröter, C. (2023). Tissue-intrinsic Wnt signals antagonize Nodal-driven AVE differentiation. *BioRxiv*, 2023.05.19.541432. https://doi.org/10.1101/2023.05.19.541432

Smith, A. (2017). Formative pluripotency: The executive phase in a developmental continuum. *Development (Cambridge)*, *144*(3), 365–373. https://doi.org/10.1242/dev.142679

Soutourina, J. (2018). Transcription regulation by the Mediator complex. In *Nature Reviews Molecular Cell Biology* (Vol. 19, Issue 4, pp. 262–274). Nature Publishing Group. https://doi.org/10.1038/nrm.2017.115

Stevens, J. L., Cantin, G. T., Wang, G., Shevchenko, A., Shevchenko, A., & Berk, A. J. (2002). Transcription control by E1A and MAP kinase pathway via Sur2 mediator subunit. *Science*, *296*(5568), 755–758. https://doi.org/10.1126/SCIENCE.1068943

Szklarczyk, D., Franceschini, A., Wyder, S., Forslund, K., Heller, D., Huerta-Cepas, J., Simonovic, M., Roth, A., Santos, A., Tsafou, K. P., Kuhn, M., Bork, P., Jensen, L. J., & Von Mering, C. (2015). STRING v10: protein-protein interaction networks, integrated over the tree of life. *Nucleic Acids Research*, *43*(Database issue), D447–D452. https://doi.org/10.1093/NAR/GKU1003

Tang, M., Kaymaz, Y., Logeman, B. L., Eichhorn, S., Liang, Z. S., Dulac, C., & Sackton, T. B. (2021). Evaluating single-cell cluster stability using the Jaccard similarity index. *Bioinformatics*, *37*(15), 2212–2214. https://doi.org/10.1093/BIOINFORMATICS/BTAA956

Tee, W. W., Shen, S. S., Oksuz, O., Narendra, V., & Reinberg, D. (2014). Erk1/2 activity promotes chromatin features and RNAPII phosphorylation at developmental promoters in mouse ESCs. *Cell*, *156*(4), 678–690. https://doi.org/10.1016/j.cell.2014.01.009

Tutter, A. V., Kowalski, M. P., Baltus, G. A., Iourgenko, V., Labow, M., Li., E., & Kadam, S. (2009). Role for Med12 in regulation of Nanog and Nanog target genes. *Journal of Biological Chemistry*, *284*(6), 3709–3718. https://doi.org/10.1074/jbc.M805677200

Villegas, F., Lehalle, D., Mayer, D., Rittirsch, M., Stadler, M. B., Zinner, M., Olivieri, D., Vabres, P., Duplomb-Jego, L., De Bont, E. S. J. M., Duffourd, Y., Duijkers, F., Avila, M., Geneviève, D., Houcinat, N., Jouan, T., Kuentz, P., Lichtenbelt, K. D., Thauvin-Robinet, C., … Betschinger, J. (2019). Lysosomal Signaling Licenses Embryonic Stem Cell Differentiation via Inactivation of Tfe3. *Cell Stem Cell*, *24*(2), 257-270.e8. https://doi.org/10.1016/J.STEM.2018.11.021

Wamaitha, S. E., del Valle, I., Cho, L. T. Y., Wei, Y., Fogarty, N. M. E., Blakeley, P., Sherwood, R. I., Ji, H., & Niakan, K. K. (2015). Gata6 potently initiates reprograming of pluripotent and differentiated cells to extraembryonic endoderm stem cells. *Genes & Development*, *29*(12), 1239–1255. https://doi.org/10.1101/GAD.257071.114

Ying, Q. L., Wray, J., Nichols, J., Batlle-Morera, L., Doble, B., Woodgett, J., Cohen, P., & Smith, A. (2008). The ground state of embryonic stem cell self-renewal. *Nature*, *453*(7194), 519–523. https://doi.org/10.1038/nature06968

Youden, W. J. (1950). INDEX FOR RATING DIAGNOSTIC TESTS. *Cancer*, *3*(1), 32–35. https://doi.org/10.1002/1097-0142(1950)3:1<32::AID-CNCR2820030106>3.0.CO;2-3

Supplementary Figures

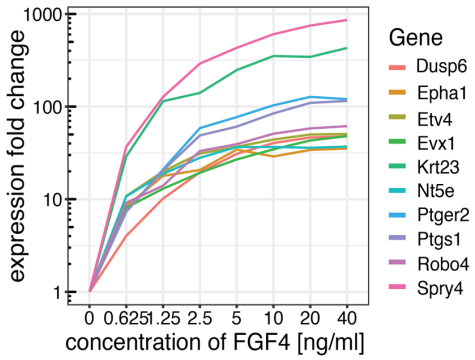

Fig. 1 Supp 1: *Spry4* is strongly upregulated upon FGF stimulation.

Expression fold change of the ten most upregulated genes upon FGF4 titration in *Fgf4* mutants. *Fgf4*-mutant *Spry4*$^{H2B\text{-}Venus/+}$ cells were transitioned from 2i + LIF medium containing 10% FBS to N2B27 supplemented with Chiron and LIF for 18 h, followed by 6 h of stimulation with indicated concentrations of FGF4 in N2B27 with Chiron.

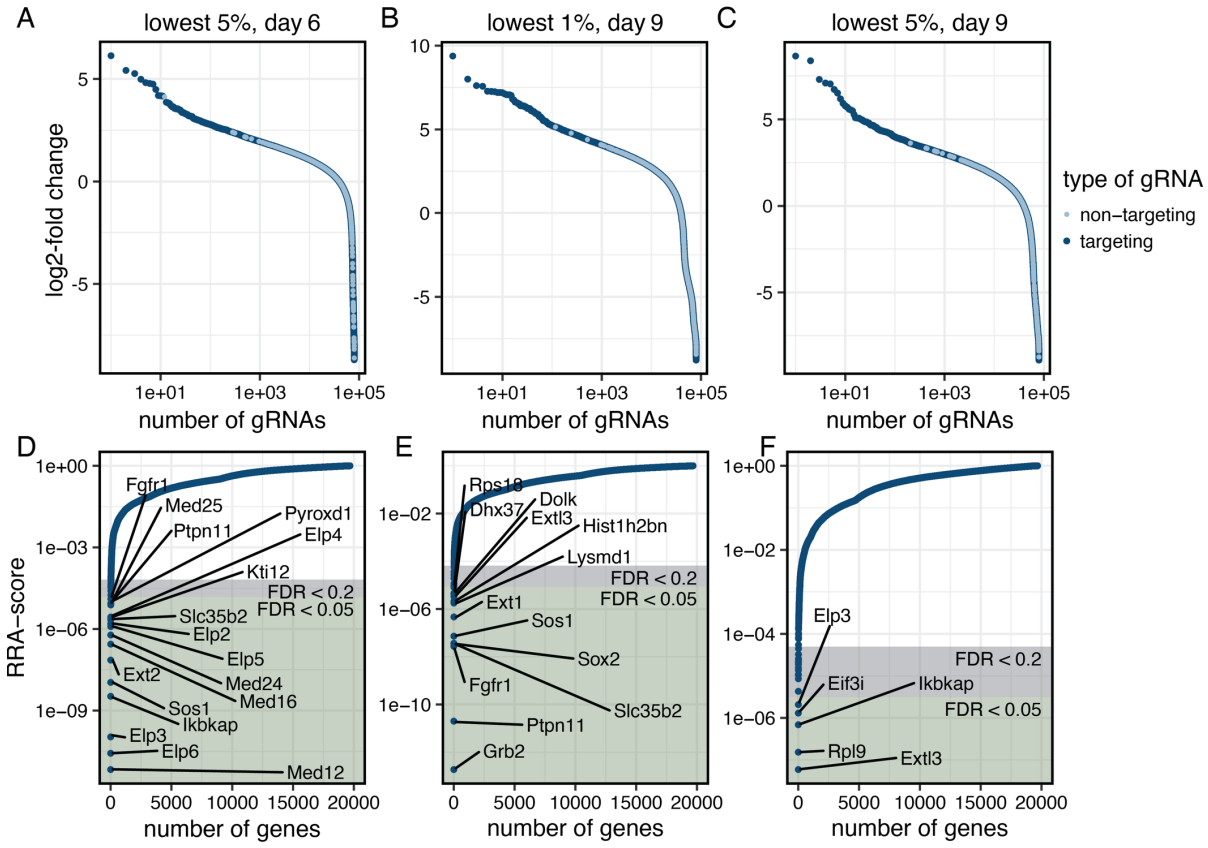

Fig. 1 Supp 2: Genome-wide CRISPR knockout screen results in robust enrichment of gRNAs and corresponding genes.

A - C Log 2-fold enrichment of gene-targeting (dark blue) and control gRNAs (light blue) in cells sorted for the lowermost 5% of H2B-Venus signal on day 6 after gRNA transduction (A), sorted for the

lowermost 1% on day 9 after transduction (B), or sorted for the the lowermost 5% on day 9 after transduction (C). **D** - **F** RRA scores for genes corresponding to enriched gRNAs identified in A - C.

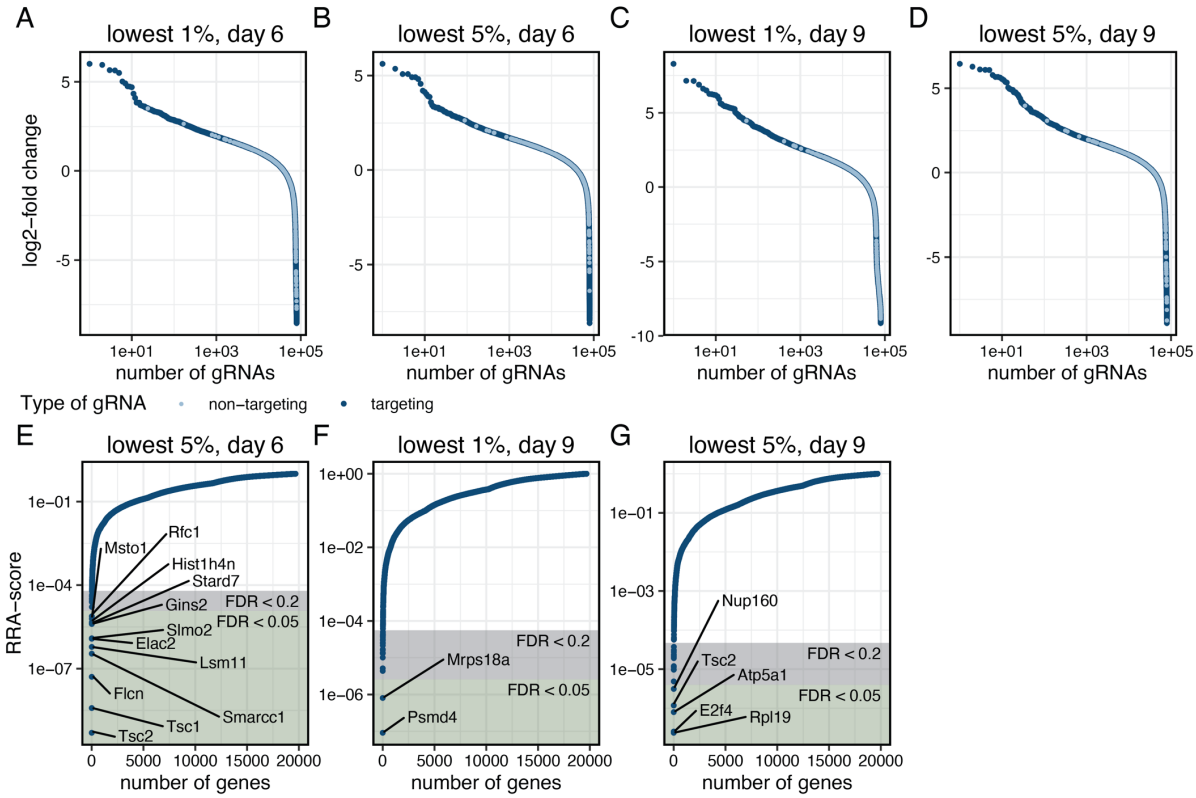

Fig. 2 Supp 1: Robust enrichment of gRNAs and corresponding genes that negatively regulate Spry4:H2B-Venus expression.

A - **D** Log 2-fold enrichment of gene-targeting (dark blue) and control gRNAs (light blue) in cells sorted for high H2B-Venus expression on different days as indicated.

E - **G** RRA scores for genes corresponding to enriched gRNAs identified in B - D. RRA scores for genes corresponding to gRNAs enriched in the 1% of the cells with highest fluorescence after 6 days are shown in Fig. 2A.

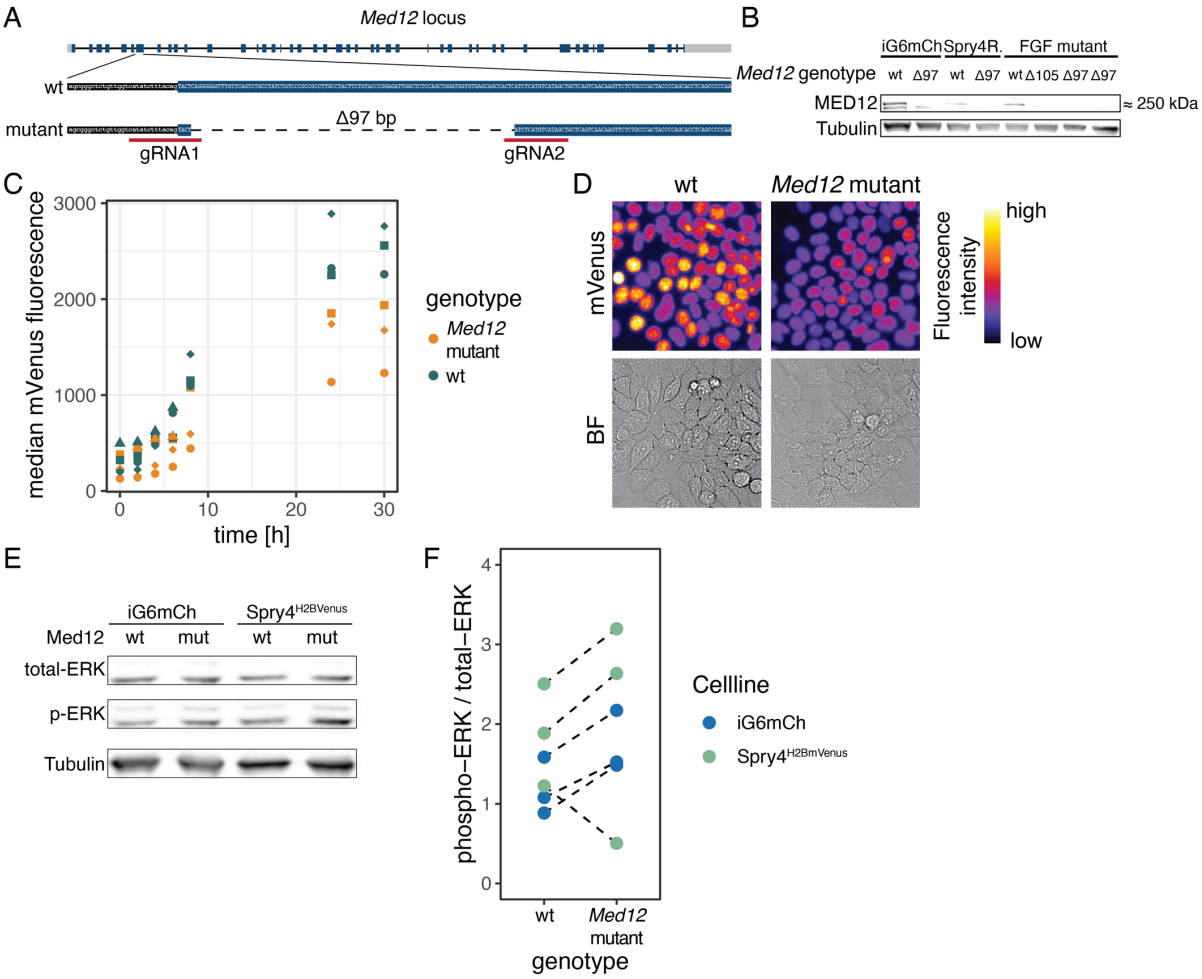

Fig. 3 Supp1: Generation of *Med12* mutant cell lines.

A Schematic of the *Med12* gene locus and the gRNAs used to create a *Med12* loss-of-function by deleting part of exon7.

B Immunoblotting of cell lysates from several monoclonal *Med12* mutant lines generated in different genetic genetic backgrounds, stained for MED12 and Tubulin.

C *Spry4*$^{H2B\text{-}Venus/+}$ Expression upon release from 2i + LIF to N2B27 in wild-type and *Med12*-mutant cells measured by flow cytometry. Data points show median fluorescence in each experiment. N = 3.

D H2B-Venus expression in live wild-type and *Med12*-mutant *Spry4*$^{H2B\text{-}Venus/+}$ cells after 24 h of growth in N2B27 following release from 2i + LIF.

E Immunoblotting of cell lysates from *Med12* wild type and *Med12*-mutant *Spry4*$^{H2B\text{-}Venus/+}$ and iGata6 mESCs, stained for Tubulin, total- and phopsho-ERK.

F Quantification of phospho-ERK signals from immunoblots, normalized to total-ERK. N=3.

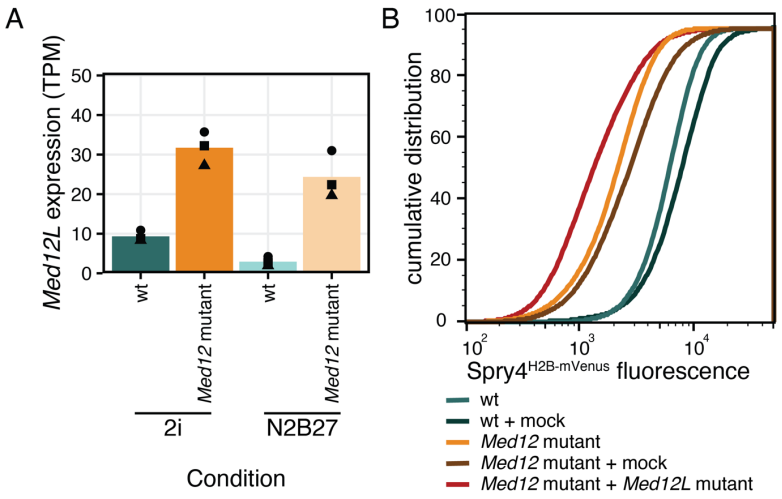

Fig. 3 Supp 2: *Med12l* is upregulated upon loss of *Med12*.

A Expression of *Med12l* in wild-type and *Med12*-mutant cells (data from RNA-seq experiment in Fig. 3A).

B H2B-Venus expression in untransfected wild-type and *Med12*-mutant cells, and after transfection with mock or *Med12l*-targeting gRNAs. Expression was measured by flow cytometry 7 d after transfection and culture in ES + LIF medium.

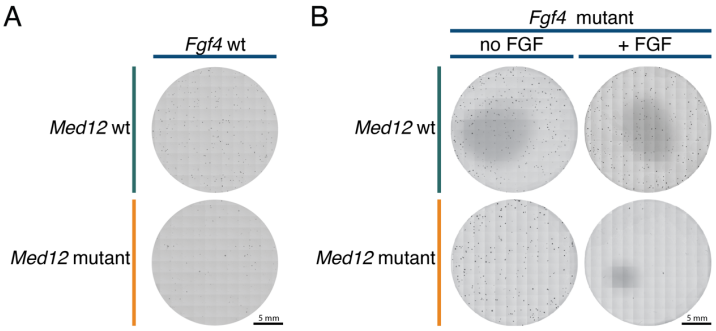

Fig. 4 Supp 1: Reduced clonogenicity in *Med12* mutants compared to wild type.

A and **B** Representative images of plates from the clonogenicity assay depicted in Fig. 4A, corresponding to quantifications shown in Fig. 4B. **A** shows plates with wild-type and *Med12*-mutant cells in an *Fgf4* wild type background, **B** shows plates with wild-type and *Med12*-mutant cells in an *Fgf4*-mutant background without (left) and with (right) FGF4 supplementation.

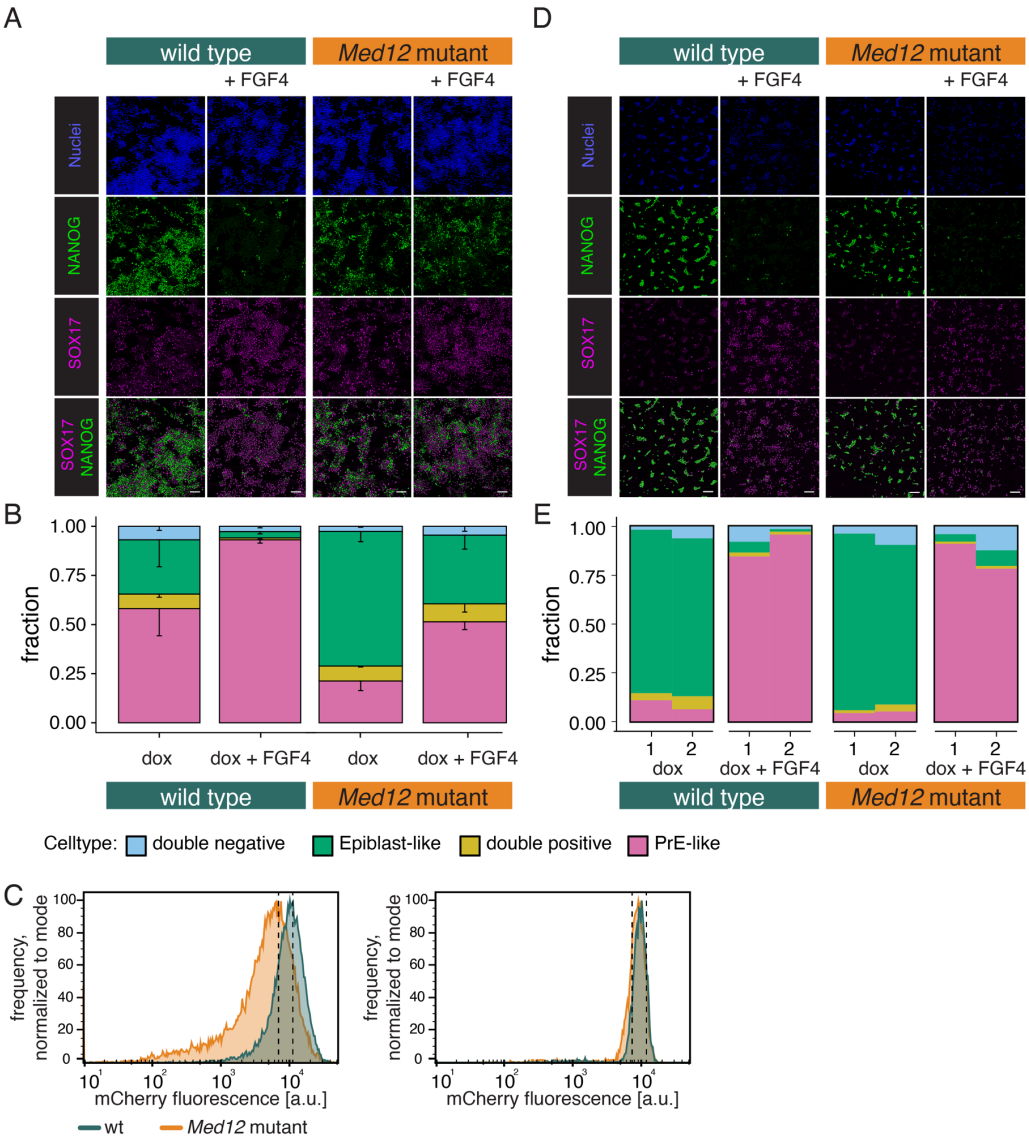

Fig. 5 Supp 1: Lower GATA6-mCherry induction levels limit PrE differentiation in *Med12* mutant cells.

A Immunostaining of the Epi-marker NANOG (green) and the PrE marker SOX17 (magenta) after 8 h of GATA6 induction and 20 h of differentiation with and without exogenous FGF4 in wild-type and *Med12*-mutant cells. Scale bar: 100 µm.

B Quantification of cell type proportions after differentiating wild-type and *Med12*-mutant cells as in (A). N=3, n > 1100 cells per replicate, error bars indicate SEM.

C Gata-mCherry fluorescence after 8 h of dox induction. Left shows distribution of expression levels in the whole population, right shows expression levels after flow sorting of cells with similar fluorescence intensity. Dashed lines indicate sorting gate.

D Immunostaining of the Epi-marker NANOG (green) and the PrE marker SOX17 (magenta) after 8 h of GATA6 induction, flow sorting as described in (C), reseeding and 20 h of differentiation with and without exogenous FGF4 in wild-type and *Med12*-mutant cells. Scale bar: 100 µm.

E Quantification of cell type proportions after differentiating wild-type and *Med12*-mutant cells as in (D). N=2, n > 500 cells per replicate.

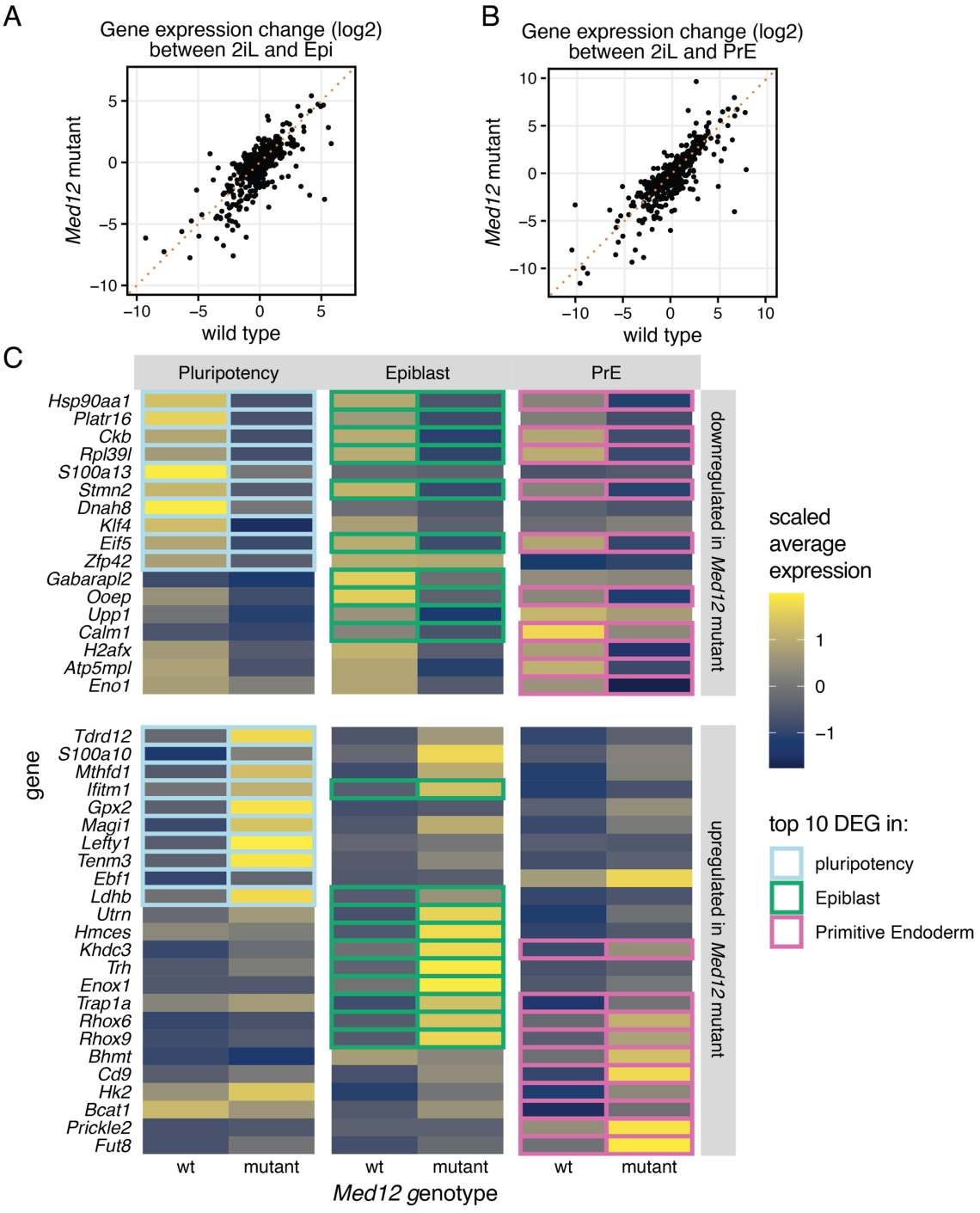

Fig. 6 Supp 1:

A and **B** Expression change of each gene upon differentiation from pluripotency (2iL) to Epi (A) and PrE (B) in wild-type versus *Med12*-mutant cells. Dotted, orange line indicates the unity line.

C Differentially expressed genes between *Med12* wild type and mutant cells for the three different cell states. Tile color shows scaled average gene expression, colored boxes indicate the 10 genes with the largest fold-change between *Med12* wild type and mutant cells in each cell state.

Supplementary Table legends

Supp Table 1: Raw and processed data from CRISPR screen including detected counts of gRNAs and enriched genes.

Supp Table 2: Differentially expressed genes comparing wild-type and *Med12*-mutant cells in 2i and after 24 h differentiation in N2B27.

Supp Table 3: Differentially expressed genes in *Fgf4*-mutant and *Fgf4 Med12* double mutant cells upon FGF4 stimulation in N2B27.

Supp Table 4: Raw and normalized counts of colonies detected in the colony formation assay.

Supp Table 5: Differentially expressed genes between the Epi- (cluster 1) and PrE-cells (cluster 0) determined by single cell RNA sequencing experiment.

Supp Table 6: Differentially expressed genes between wild-type and *Med12*-mutant cells separately in pluripotency conditions, the Epi- and PrE-cluster.

Supp Table 7: Oligos used as gRNAs or PCR primers.

Supplementary Movie legends

Supp Movie 1: Timelapse imaging of H2B-Cerulean (blue) and iGata6-mCherry expression (red) in wild-type and Med12-mutant cells during Epi and PrE differentiation under same conditions as in Figure 3E. Following time lapse imaging, cells were immunostained for the Epi-marker NANOG (green) and the PrE marker SOX17 (magenta). Nuclei in immunostainings labelled with Hoechst dye (cyan). Scale bar: 50 µm.